Chapter 7
Building Laboratory Superconducting Magnets

Abstract This chapter gives tips to the researchers how to design, build and operate standard superconducting solenoid magnets in the laboratory and use them for physical property measurements. Broad parameters discussed are the design dimensions, homogeneity, current lead optimization, current supply, quench protection and persistent switches. Multifilamentary Cu/Nb–Ti conductor is the universal choice for building (multi-section) magnets producing field up to 8 T (4.2 K). Additional field is produced by using inserts of A-15 Nb_3Sn conductor, usually of the 'wind and react' type. Specific examples of the design, fabrication and operation of a 7 T Nb–Ti magnet, a 11 T Nb–Ti/Nb_3Sn combination magnet and a 6 T cryofree magnet, built in author's laboratory, have been discussed. Delicate steps followed during winding, tension adjustment, controlled high temperature reaction, preparation of current contacts and the final impregnation of the Nb_3Sn magnet have been elaborated. The chapter presents all salient features of a superconducting magnet and the latest developments made in achieving record fields in conventional and HTS magnets.

7.1 The Solenoid Magnets: Introduction

The fact that superconductors carry current without dissipation, has made them ideal for building magnets. A magnet coil is, however, a common component of any electro-technical machine. Attempts have been continuously made to develop superconductors that can produce higher and higher magnetic field. The motivation to produce high magnetic field has come from such diverse applications as listed below.

R.G. Sharma, *Superconductivity*, Springer Series in Materials Science 214,
DOI 10.1007/978-3-319-13713-1_7

- Magnetic field is a versatile thermodynamic parameter like pressure and temperature which can manipulate phase diagram of magnetic materials wherein electrons spins can order ferro or antiferromagnetically and alter the behaviour of a material.
- Magnetic field is an essential tool for scientific research in several disciplines like condensed matter physics, material science, atomic and molecular physics, life sciences and chemistry. Whenever the field was raised by a significant step, a new phenomenon was discovered or a high precision device built.
- High magnetic field enables the observation of Quantized Hall Effect (QHE) and Fractional Quantum Hall Effect (FQHE) in quantized electron energy levels. QHE is already in use internationally for resistance standard.
- Unprecedented field stability and very high fields available with superconducting magnets has made high resolution Nuclear Magnetic Resonance (NMR) spectroscopy a powerful tool to study structure of large and complex molecules. 1 GHz NMR spectrometers (23.5 T field) are now commercially available (Fig. 10.6).
- Whole-body Magnetic Resonance Imaging (MRI) based on NMR principle is extensively used in non-destructive and non-invasive imaging of living systems. Magnetic Resonance Imaging (MRI) has become an important diagnostic tool with radiologists and has benefited the society at large.
- Superconducting magnets are playing pivotal role in high energy particle accelerators and fusion reactors. The success of Large Hedron Collider (LHC) can be attributed to a large extent to superconducting magnets. The success of on-going projects like International Thermonuclear Energy Reactor (ITER) and International Linear Collider (ILC) too is equally dependent on the perfection to which the magnets will be built.

7.2 A Brief History of Superconducting Magnets

Kammerlingh Onnes realized the importance of superconducting materials for producing high magnetic field soon after the discovery of superconductivity but his dream of producing high field using Pb-wire remained unfullfilled because of the inherent limit of low critical field, B_c of this material. The first superconducting magnet was built at Physics Laboratory in Leiden Uni. by winding Pb wire (Fig. 7.1a) but the results were too disappointing. Magnets became a possibility in mid 1950s after the discovery of type II superconductors with high upper critical field, B_{c2} values. Yntima [1] built a successful superconducting magnet for producing low temperature by adiabatic demagnetization of a paramagnetic salt. He wound a fine enameled strained Nb-wire (dia. 0.05 mm) over a soft iron core and produced a field of 0.7 T in a pole gap of 2.78 mm. The number of turns of Nb-wire were 4,296. The Nb layer was covered by another layer, that of the bare Cu wire of 0.46 mm diameter, having 183 turns. He wound magnets using cold-worked as well

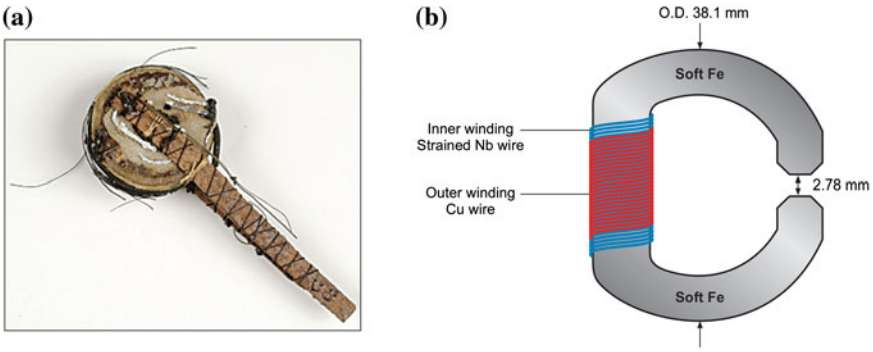

Fig. 7.1 **a** World's first superconducting magnet wound with Pb-wire at Leiden Physics Laboratory in 1912. *Image Courtesy* of Museum Boerhaave, Leiden, The Netherlands (2011) http://www.aps.org/meetings/march/vpr/2011/imagegallery/supercoil.cfm. **b** World's first successful superconducting magnet wound by Yntima using strained Nb-wire at Uni. of Illinois in 1954 producing a field of 0.71 T (adapted and modified from [1])

as annealed Nb-wires and found that cold-worked wires carry larger current compared to annealed wires and produce higher field. This was perhaps the first indication that defects introduced in superconductors enhance the critical current via the mechanism of flux pinning.

An important event was the development of a 9.2 T magnet by Coffey et al. [2] using three sections of Nb–Ti wire in a background field of 5 T provided by two-section Nb–Zr coil. High field superconducting magnets, however, became possible only after the discovery of A-15 superconductors. The year 1961 proved to be a turning point in the history of superconducting magnet development when Kunzler et al. [3] at Bell Lab showed conclusively that field in excess of 10 T were possible using Nb_3Sn conductor. Nb_3Sn magnets in pancake structure were built using flexible tapes of Nb_3Sn deposited on hastelloy tapes either by Sn-diffusion technique or the chemical vapour deposition (CVD) technique in 1960s. These magnets were, however, not stable against flux jumps. The emergence of Cu-stabilized multifilamentary (Nb–Ti and Nb_3Sn) wires and cables in 1970s laid a strong foundation for real high field superconducting magnet technology. Continuous improvement in the J_c values of Nb_3Sn conductor through improved mechanical deformation techniques and metallurgical processing has led to an all time high magnetic fields. Multi-section (Nb–Ti/Nb_3Sn) magnets producing 20 T field are commercially available. The use of HTS (Bi-2223 or 2G YBCO) inserts has pushed this value to still higher fields in excess of 22 T. A 32 T superconducting magnet has been designed, fabricated and tested at NHFML, Florida State University [4, 5]. The magnet uses two sections of Nb–Ti, and three sections each of Nb_3Sn and YBCO conductors. Other advances in producing very intense field have recently been made at BNL and NHFML, BNL produced a field of 16 T by a REBCO stand alone magnet. NHFML generated a record field of 35.4 T [6] using a REBCO insert in a background field of 31 T provided by a resistive 20 MW magnet. The insert contributed a field of 4.4 T.

During last decade and a half 'conduction-cooled' or 'cryo-free' superconducting magnet systems have flooded the research laboratories which do away with the use of liquid helium for magnet cooling. Instead, the magnet system is cooled by closed cycle refrigerators (CCR). This has been possible for two reasons. One, that CCR of 1.5 W cooling @ 4 K are commercially available and second, that HTS current leads capable of carrying thousands of Ampere current have been commercialized. Superconducting leads do not generate Joule-heating and have poor thermal conductivity. Cooling need of the magnet system is comfortably met with the CCRs. Cryo-cooled magnets capable of generating high field up to 20 T have found their way in research laboratories. These magnets are hooked-up with a large variety of physical and magnetic measurement systems.

7.3 Unique Features of a Superconducting Magnet

The winding of a superconducting magnet is quite an intricate exercise because of the peculiar behaviour of a superconductor carrying large current in high magnetic field and the large mechanical forces encountered by the conductor. We discuss below some of these peculiarities.

- In a superconducting magnet the magnet current is a function of temperature and the magnetic field. The maximum current that a coil can carry depends upon the maximum field experienced by the superconductor. The operating temperature for most magnets is 4.2 K provided by liquid helium bath. For enhanced fields the magnet is operated at a reduced temperature of 1.8 K.
- Superconducting wires are produced in the form of multifilaments embedded in high conductivity copper by a multi-step process. This is needed to overcome stability problems, discussed in detail in Sect. 6.2.
- The magnet wire is subjected to mechanical load primarily due to winding tension and the bending strain.
- Differential thermal contraction of the constituent materials of the magnet gives rise to stress when cooled to operating temperature.
- There is stress internal to the conductor because of the sharp change of temperature from reaction temperature to operating temperature.
- Since these magnets generate strong fields the conductor experiences large radial Lorentz force which gives rise to hoop stress (=BJR) which can be severe in large size magnets.
- The J_c of superconducting wires has a very strong stress-strain characteristic. Strain under load can bring down J_c drastically.
- Any micro-movement of the conductor under large Lorentz force can generate heat sufficiently high to drive the conductor to normal state and quench the magnet. To prevent such movement of the conductor the magnet is always impregnated with a suitable low temperature compatible epoxy or bees wax.

- The magnet is always susceptible to quench for a variety of reasons such as insufficient cooling, exceeding the current beyond J_c, too high current ramp rate or for any unforeseen thermo-mechanical disturbance. During the quench, the stored energy of the magnet (=½ LI^2) released can burn the magnet. This energy therefore has to be dumped outside of the magnet. A fool-proof quench protection system is therefore integrated with the superconducting magnet to save it from burn-out.
- Notwithstanding the extreme care that is needed to build superconducting magnet systems, the magnet industry has seen an unprecedented growth over last five decades. This is because of the distinct advantages these magnets have over the normal copper-iron electromagnets. Since iron core in a normal electromagnet saturates at around 2 T, superconducting magnets are indispensable when intense magnetic field is required. These magnets are very compact, occupy little space, are light in weight and consume very little energy. No elaborate water cooling system is required either. Superconducting magnets are traditionally operated in liquid helium bath but small size magnets are increasingly cooled by cryocoolers.

7.4 Design Considerations of a Solenoid Magnet

An excellent paper on the method of optimization of winding parameters of a superconducting solenoid magnet has been published by Boom and Livingston [7] as early as in 1962. The calculation method is based upon the classical theory of Fabry [8, 9]. Quite a few good books [10–14] too have been published at different times which have been serving the community well for designing and constructing laboratory superconducting magnets for almost all types of applications. Several computer programmes for different applications are available for various aspects of magnet design.

Superconducting magnets widely used for research are almost exclusively solenoids. It will therefore be most appropriate if we describe the design of such a magnet in detail. Let us consider a solenoid as shown in Fig. 7.2 with a working bore $2a_1$, outer winding dia. $2a_2$ and the winding length 2ℓ. The current I produces a central field B_0 and a maximum field, B_M close to the inner winding layer.

The axial field of an infinite length solenoid is given by

$$B_0 = J\,\lambda\,a_1 F(\alpha,\,\beta) \tag{7.1}$$

where B_0 is the axial field in the mid-plane, J the current density of the conductor, λ the space factor (total conductor cross section divided by the total winding cross section), $\alpha = a_2/a_1$, the ratio of the outer winding diameter to inner winding diameter, $\beta = 2\ell/2a_1$, the ratio of the winding length to inner winding diameter and $F(\alpha, \beta)$ is a geometry dependent quantity called field factor, shape factor or Fabry parameter and is given by

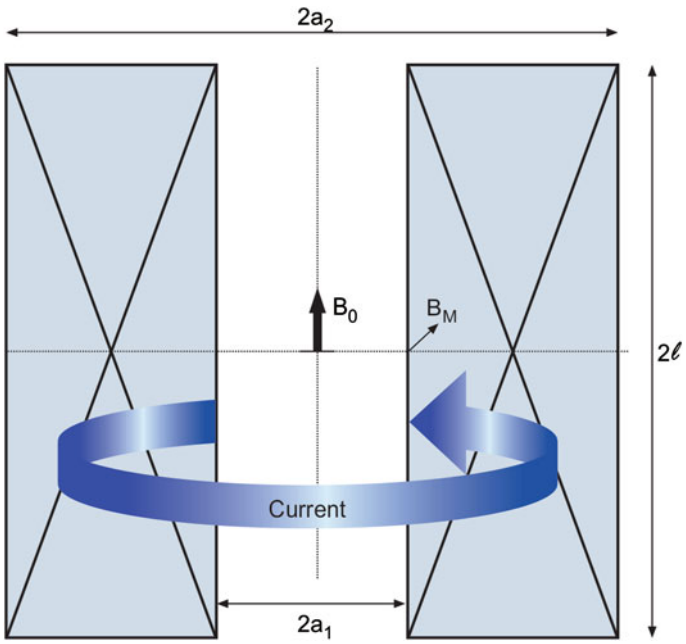

Fig. 7.2 A solenoid magnet of inner dia. $2a_1$, outer dia. $2a_2$ and a winding length 2ℓ. The axial field is B_0 and the maximum field B_M at the innermost winding layer

$$F(\alpha, \beta) = \mu_0 \beta \ln \left[\frac{\alpha + \left(\alpha^2 + \beta^2\right)^{1/2}}{1 + \left(1 + \beta^2\right)^{1/2}} \right] \tag{7.2}$$

To start designing a solenoid magnet, we select the working bore and then the inner winding dia. $2a_1$, after taking the thickness of the former into account. We then select the central axial field, B_0. The current density J is found out from the I_c-B plot of the conductor intended to be used. λ usually varies from 0.7 to 0.9 depending upon the voids in the winding and non-superconducting stuff such as interlayer insulation etc. used. The value of field factor, $F(\alpha, \beta)$ is now determined. Interestingly, for one value of $F(\alpha, \beta)$ several combinations of α and β are possible to yield the same field as shown in Fig. 7.3. It is possible to choose a combination values of α and β which corresponds to the minimum winding volume. Unfortunately, this geometry leads to a short and fat coil which in turn leads to a poor field homogeneity and consume more conductor. For high field homogeneity we must select parameters α and β away from minimum volume condition using larger value of β. The maximum axial field is experienced on the inner most layer of the winding. It is this field which ultimately restricts the operating current of the magnet and not the central field. In Fig. 7.4 we have plotted the maximum field experienced by the conductor at the inner most layer, B_M for a central field of 6 T and for

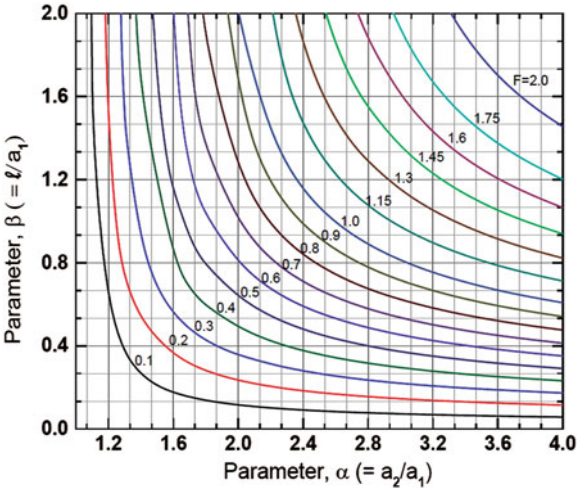

Fig. 7.3 Febry parameter, $F(\alpha, \beta)$ *curves* plotted as a function of α and β. Several combinations of α and β are possible for a given value of $F(\alpha, \beta)$ and thus for a magnet to produce a particular field (*Courtesy* Soumen and Vijay)

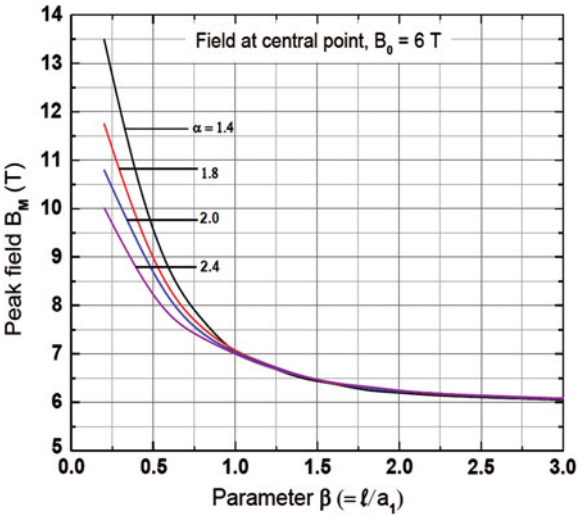

Fig. 7.4 Peak field B_M versus β plots for different values of α = 1.4, 1.8, 2.0 and 2.4 for a 6 T magnet. Field homogeneity improves with increasing β and appears to saturate beyond β = 3 (*Courtesy* Vijay, Phaneendra and Soumen)

different values of α(=1.4, 1.8, 2.0 and 2.4). Boom and Livingston [7] have plotted the homogeneity curves represented by the ratio, $k = B_M/B_0$ (ratio of peak field to the central field) as a function of α and β. It is clear from the figure that for high homogeneity one has to choose α and β values such that the B_M/B_0 ratio is as close to 1 as possible. This means β has to be much larger than that given by the minimum volume criterion. This is clearly seen from Fig. 7.4 that for a 6 T axial field the peak field rises sharply for β values less than 1 for all values of α. The peak field is reduced for β greater than 1 and becomes close to the central field B_0 for β = 3. Such a magnet will consume lesser quantity of conductor and yield high homogeneity. This results from the fact that the maximum field or the peak field is

now much reduced and the magnet can be operated at a higher current producing higher field. The central axial field B_0 increases as we move away from the centre along the radius, becomes maximum (B_M) close to the inner most winding layer and decreases thereafter and even becomes negative close to the outer edge of the winding. This means that a smaller operating magnet current is now chosen corresponding to B_M instead of the central field B_0. Since the outer layers of the winding are exposed to decreasing field, the conductor is capable of carrying much larger current than the inner part of the winding. It is therefore advisable to wind the magnet in multi-sections, outer sections operating at larger current densities than the inner ones. Better still, if we use different dia. wires in different sections and run them at the same current, that is, at different current densities as dictated by the J_c-B plots of the conductor. Such a magnet will consume lesser quantity of conductor and yield high homogeneity. This results from the fact that the maximum field or the peak field is now much reduced and the magnet can be operated at a higher current producing higher field. One should therefore use thicker wire for the inner and thinner wire for the outer sections. We built several 7–8 T Nb–Ti magnets in two sections using 0.75 mm dia. wire for the inner section and a 0.54 mm for the outer section and running them in series using the same current supply.

7.4.1 Specific Example of a 7 T Superconducting (Nb–Ti) Magnet

Let us take an example of designing a 7 T Nb–Ti magnet to be used as an insert to a 100 mm neck dia. liquid helium storage vessel [15]. To keep the outer diameter of the magnet smaller than 100 mm (LHe-vessel neck dia.) we chose a thicker Cu/Nb–Ti wire (0.75 mm dia.) and a high operating current $\sim$210 A. We started with a former of clear bore of 46 mm and the inner winding dia. ($2a_1$) of 50 mm. We used a 45 filament Cu/Nb–Ti wire supplied by Vacuumschmelze. This wire had an I_c = 245 A at 7 T field and we take 85 % of this value, that is 208 A as the operating current. λ, the space factor is taken to be 0.78, a value we find consistently in many of our magnets wound using a fiber-glass cloth as inter-layer material. J is obtained by dividing 208 by area cross-section of the wire (0.4418×10^{-6} m^2) which turns out to be 470×10^6 A m^{-2}. By putting the appropriate values in (7.1) the function F (α, β) comes out to be 0.76255×10^{-6} for a field of 7 T. Using the B_M/B_0 plots for different combinations of α and β in Fig. 3.3 of Wilson [12] we selected a ratio k (B_M/B_0) to be 1.0112 such that the peak field at the inner winding layer is just 7.078 T low enough to allow a safe operating current of 208 A. We now select from the same figure a combination of α = 1.665 and β = 3 compatible with this field ratio. Thus the outer winding diameter of the coil, $2a_2$ becomes = 83.25 mm and the winding width = 16.6 mm. Since β is to be 3 a winding length 150 mm has been chosen. One layer will have 200 turns and there will be 22 layers in all. The total number of turns thus becomes = 4,400. The parameter details of the magnet are reproduced in Table 7.1.

The former was made out of SS and a layer of fiber glass cloth was wrapped on the bare surface of the former before starting winding. Thin G-10 sheets were fixed on the inside of the two SS end flanges. The flanges and the central pipe of the former had perforations to allow LHe to seep and cool the winding. The wire terminals were taken out through the top end flange at an easy slop. A schematic diagram of the former and the winding is shown in Fig. 7.5. Winding was carried out on a modified lathe with 0.75 mm pitch and rotating at a comfortable speed of 18 rpm. Each layer was very tightly wound and had 200 turns. A tension of 1 kg was uniformly maintained throughout the winding. To prevent possibility of wire movement under Lorentz force during operation of the magnet precaution should be taken not to leave gap in the winding. We always wind an even number of layers so that the second terminal of the wire can also be taken out from the top flange. After the winding, the two terminals of the wire were secured in position and the magnet was vacuum-pressure impregnated in bees wax.

The magnet was suspended from a top flange using G-10 supports and radiation shields. Two vapour cooled optimized current leads also terminate at the top flange for connecting with the power supply. Figure 7.6a shows the bottom part and Fig. 7.6b the top part of the magnet assembly. A relief valve is provided at the top flange for He-gas to escape in the event of a pressure build-up in the LHe vessel. Helium gas flow through the current leads is regulated using a control valve which is connected to the recovery line. A He-gas flowmeter, in the gas recovery line measures the He-gas evaporation rate. The magnet assembly pre-cooled with liquid nitrogen is gently and slowly lowered into the LHe-storage vessel and experiments can be performed rather quickly as compared with conventional magnets operated in dedicated LHe-dewars which need time to be ready for operation.

Table 7.1 Parameters of the 7 T solenoid magnet of insert type

Parameter	Value	Parameter	Value
Working bore	46 mm	Conductor used	Cu/Nb–Ti (MF)
Inner winding dia. $2a_1$	50 mm	Cu:Nb–Ti	1.8:1
Outer winding dia. $2a_2$	83.25 mm	Conductor dia.	0.75 mm
Winding width w	16.6 mm	No. of filaments	45
Winding length, 2ℓ	150 mm	Filament dia.	38 μm
Parameter α	1.665	Inductance	0.4 H
Parameter β	3	Field at 208 A	7 T
Function $F(\alpha, \beta)$	0.76255×10^{-6}	Field factor	29.71 A/T
Field homogeneity	0.094 % (10 mm DSV)	Quench field at 210 A	7.1 T
No. of layers	22	Stored energy at 210 A	8.8 kJ
Total no. of turns	4,400	Impregnating material	Bees wax
Conductor length	0.9 km	Inter-layer material	Fiber glass cloth

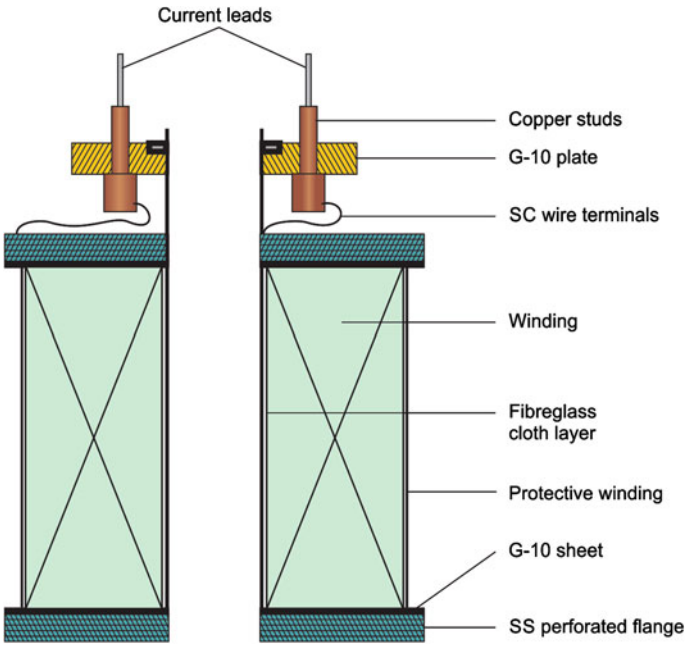

Fig. 7.5 Schematic diagram of the former and the winding of a 7 T magnet of the insert type

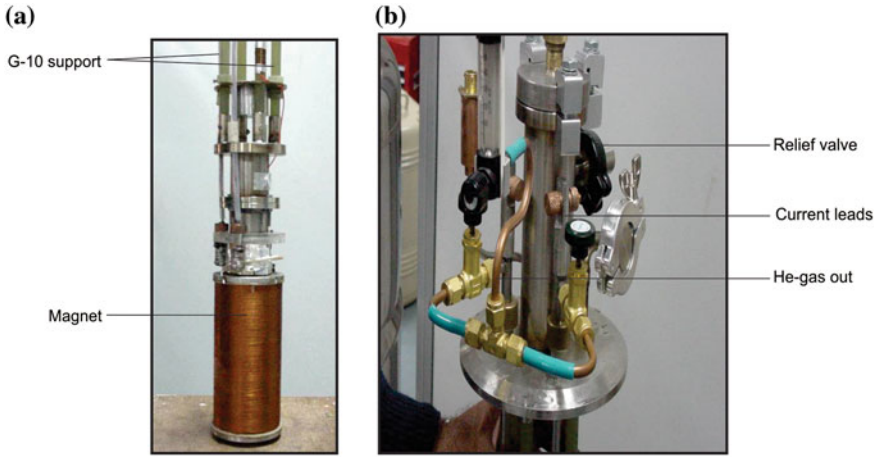

Fig. 7.6 **a** The 7 T magnet and the *bottom* part of it's support system. **b** *Top view* the flange, seen in the picture fits on to the *top* of the LHe-vessel neck, He-gas flows through the current leads and is collected via a gas flow meter [15] (*Courtesy photo* IUAC Delhi)

The axial field variation with the distance from the mid-plane is plotted in Fig. 7.7. The inset shows the axial field homogeneity of 0.098 % in a 10 mm DSV (diameter spherical volume). The radial component of the axial field along the axis remains zero.

Figure 7.8 shows the plots of the magnetic field lines using Poisson Superfish computer programme. Three distinct features can be noted from this figure. First, that the density of magnetic field lines increases as one moves away from the mid plane along the radius of the magnet. It becomes maximum at the inner-most winding layer. It is for this reason, that the axial field peaks at the inner winding layer. Second, that the density of lines of force decreases thereafter and becomes zero close to the outermost layer. The zero-field region is indicated in the figure. Thirdly, the lines of force bend near the ends of the magnet, (this is true for any finite length solenoid as ours) and reverses the field direction beyond the outer most layer. The Lorentz force, generated by the interaction of perpendicular current and magnetic field ($B \times I$), at the outer layer will therefore reverse the direction and will tend to compress the coil from outside. There is already a Lorentz force acting on the inner-most layer compressing the coil. As one moves away along the radius this force decreases and then changes direction. Bending at the ends also introduces a radial component of the field which produces an axial Lorentz force tending to compress the coil axially. A magnet is therefore like a pressure bottle similar to a high pressure gas cylinder trying to explode. This pressure is $=B^2/2\mu_0$ and for a field

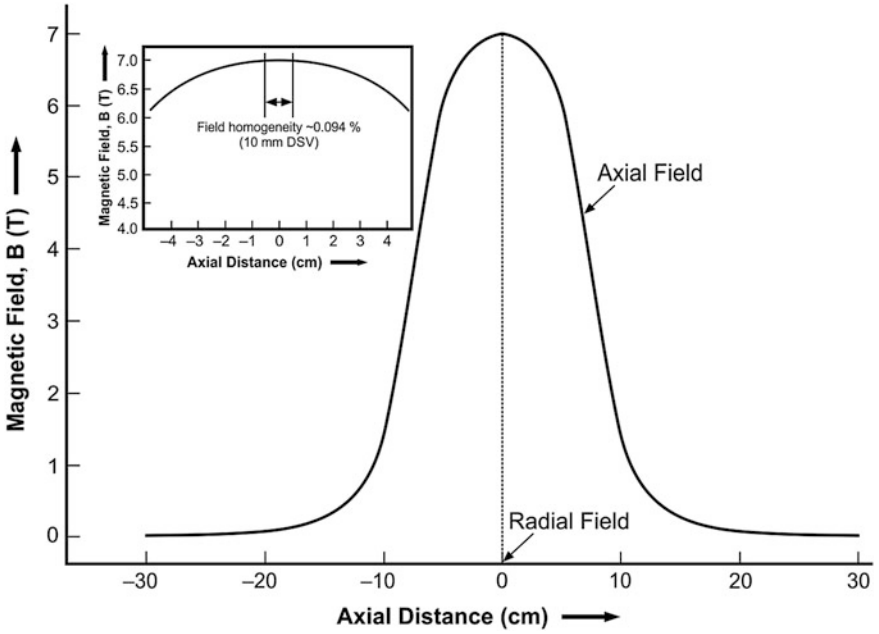

Fig. 7.7 The axial field profile of the magnet at 7 T. The inset shows a field homogeneity of 0.098 % in a 10 mm DSV. The radial field along the axis is nearly zero [15]

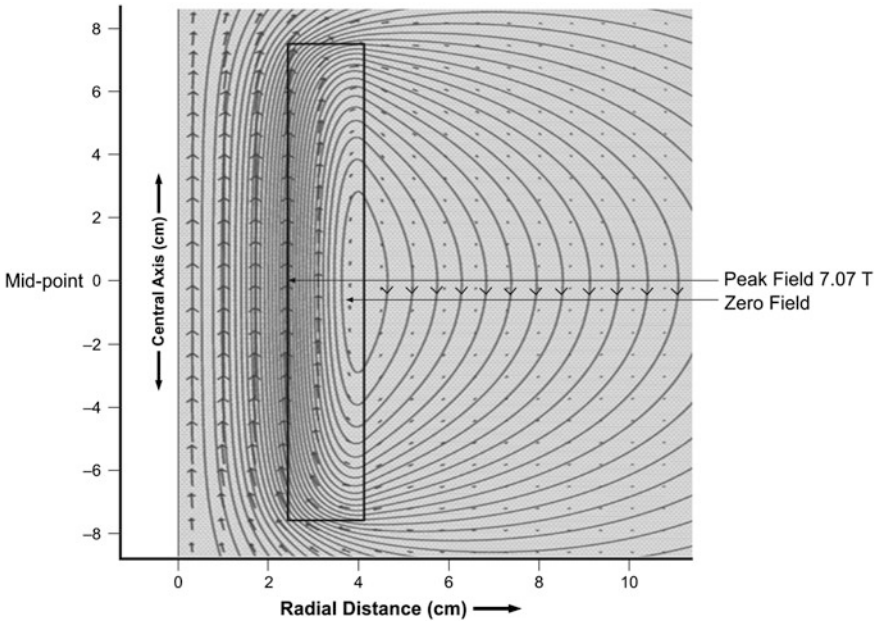

Fig. 7.8 Field profile of the 7 T magnet plotted by using Poisson Superfish computer programme. Note the peak field region and the zero field region [15]

value of 10 T it turns out to be as high as 4×10^7 N/m^2 which is close to the yield strength of copper. Large Lorentz force also gives rise to large hoop stresses tending to explode the magnet. Reinforcement of the magnet-winding is thus extremely important. The fact that peak axial field occurs at the inner most layer, implies that the critical current density, J_c of the conductor chosen should be with respect to this field and not the field at the centre.

7.4.2 Optimization of Vapour-Cooled Current Leads

The current lead is a critical component of a superconducting magnet system in so far as it is the biggest source of heat leak to the LHe-bath. The current lead carries large current and consequently generates large amount of Joule heat. This heat is transported to He-bath. Heat is also transported from the top plate at room temperature to the bath though the leads by thermal conduction. The dimensions of the current leads can, however, be optimized for a given current such that the heat leak to the bath is minimum. Copper current leads have been universally used because of its being a good electrical conductor. Paradox, however, is that any good electrical conductor also happens to be a good conductor of heat. The thermal conductivity (k) and the

electrical resistivity (ρ) of a metal are related through the Weidemann- Franz Law, namely $k_{(T)}\,\rho_{(T)} = L_0 T$ where L_0 is the Lorenz number = 2.45×10^{-8} WΩK^{-2}. So it does not matter what material one chooses for current leads, SS or copper. In SS the Joule heating will be very high but heat conduction to the bath will reduce, SS being a poor thermal conductor of heat. In copper leads it will be just reverse, that is, Joule heating will reduce but thermal conduction will be very high. The length and cross section of the leads are optimized such that heat leak is reduced to minimum for a given lead current. Once the length of the current lead is chosen it is the cross section of the leads which is determined through the optimization procedure. The heat transport to the bath will, however, increase for smaller or higher operating current. To reduce the heat leak further, evaporated out-going helium vapours are used to cool the current leads. As shown in Fig. 7.9 the He-vapours from the cryostat are forced to flow spirally past the copper leads encased in a SS tube. The annular space between the leads and tube is packed with fiber glass roving to create fine multiple channels for efficient heat exchange.

Optimization of the current leads is done using steady state energy balance equation:

$$\frac{\mathrm{d}}{\mathrm{d}x}\left[k(T)A\frac{\mathrm{d}T}{\mathrm{d}x}\right] - \mathrm{f.m.}C_{\mathrm{P}}\frac{\mathrm{d}T}{\mathrm{d}x} + I^2\frac{\rho(T)}{A} = 0 \tag{7.3}$$

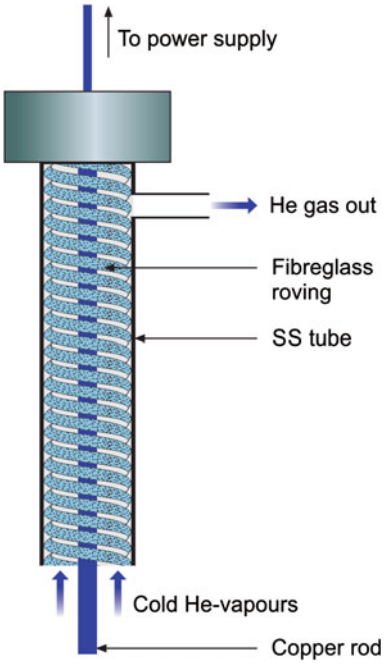

Fig. 7.9 The schematic design of the vapour-cooled current leads [15]

where A is the area cross section of the lead, C_p the specific heat at constant pressure and can be assumed constant, f is the efficiency of the heat transfer between the leads and vapours, I, the operating current and m (kg/s) the mass of liquid helium boil off by the heat leak from the lead. We optimized the leads with cross Section 0.3 cm^2 and length 75 cm for a current of 200 A. For our shape factor $(IL/A) = 3.5 \times 10^6$ A/m the minimized heat leak through the current lead comes out to be 1.04 mW/A. Thus the total heat flow to the He-bath by the two current leads at 200 A current turns out to be 0.4 W. The flow rate of the He-gas escaping from the top of the magnet system is regulated through a valve depending upon the lead-current. He-gas coming out of the top flange is found to be at room temperature establishing the efficacy of our optimization calculations.

7.4.3 Magnet Quench

Quench is a term used for a superconducting magnet when, all of a sudden, it turns normal (resistive) during the operation. This transition from superconducting state to normal state invariably occurs whenever any of the three parameters, temperature, magnetic field or current exceeds its critical value. This happens even if a minute part of the winding becomes resistive. The Joule heating (I^2R) across this resistive part will spread rather fast to the entire winding turning the magnet normal and dumping the stored energy ($\frac{1}{2}LI^2$) into the LHe-bath. This heat evaporates large amount of liquid helium and raises the temperature of the magnet far above the bath temperature. In extreme cases this dissipation of energy can burn the magnet. The occurrence of quench can, however, be minimized by stabilizing the magnet through a careful design and winding. The conductor therefore is chosen with appropriate filament size and Cu:SC ratio.

One can comfortably prevent quench caused by excessive current or poor cooling by keeping the current below the critical limit and maintaining LHe-level. The tricky part is the quench caused by the micro movement of the conductor in the winding under the influence of large Lorentz forces and by the release of strain energy. It will happen even if enough precautions are taken during winding. The quench is quite common due to wire movement during the virgin run. Let us consider a small heat pulse in the conductor in a very small part of the conductor. The heat will travel through a conductor longitudinally in both the directions at a rate determined by its thermal conductivity. We can assume near negligible dissipation in transverse direction because of inter-layer insulation and thermal contact resistance etc. If the heat dissipation from the ‘hot spot’ is faster than the generation of heat the normal zone will collapse and the magnet will be stable. If the heat dissipation is slower, the normal zone will grow and spread throughout the winding thus quenching the magnet. Interestingly, the time scale involved in quench are in the range of μ and m s. In fact, there is a critical size of the normal zone, called as minimum propagation zone (MPZ) for a given conductor which will initiate quench. This is discussed in the next section.

7.4.3.1 The Minimum Propagating Zone

To understand the concept of minimum propagating zone (MPZ) let us consider a superconductor of area cross section A carrying a current at a density J generates heat Q_{gen} due to some disturbance and raises the temperature locally of a small length ℓ to a value above T_c. turning it normal. The MPZ area and the temperature profile are shown in Fig. 7.10. The heat generated over a short length, ℓ, will travel through the superconductor longitudinally in both the directions. The heat generated in this normal region (I^2R) due to Ohmic heating will be

$$Q_{\text{gen}} = J^2 A\, \ell\, \rho \tag{7.4}$$

where ρ is the resistivity of the superconductor in normal state. This heat will travel along both the directions at a rate determined by the thermal conductivity of the normal region.

Thus the heat dissipated away Q_{Diss} will be, determined by the thermal conductivity of the normal region.

$$Q_{\text{Diss}} = 2\,k\,A\,(T_c - T_B) \tag{7.5}$$

Here k is the thermal conductivity of the conductor and T_B the bath temperature. The factor of 2 enters because of the heat being dissipated in two directions. Under

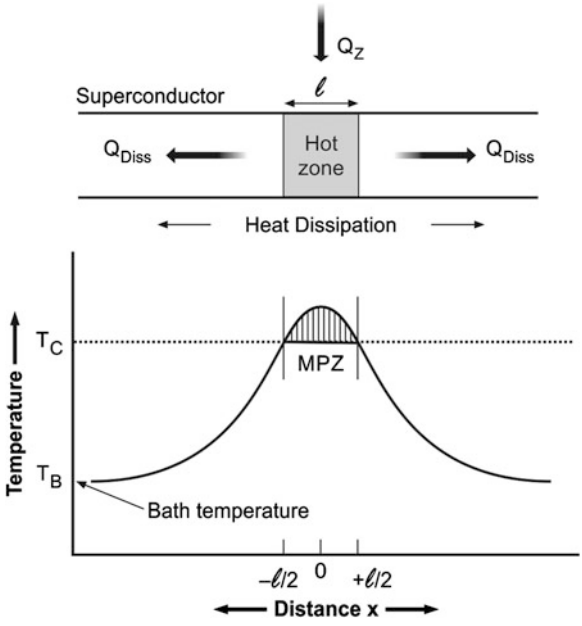

Fig. 7.10 The concept of minimum propagation zone (MPZ) and the temperature profile

equilibrium condition the two equations can be equated and we get the expression for ℓ as;

$$\ell = \left[\frac{2k(T_c - T_B)}{J^2\rho}\right]^{\frac{1}{2}} \tag{7.6}$$

If the size of the hot zone is less than ℓ, heat generated will dissipate away and the hot spot will disappear but will grow if the size exceeds ℓ.

To have an idea of the magnitude of MPZ in Nb–Ti, let us assume a $J = 4 \times 10^8$ A m^{-2}, T_c (6 T) = 6.71 K, T_B = 4.2 K, the electrical resistivity, $\rho = 6.5 \times 10^{-7}$ Ω m and thermal conductivity, $k = 0.1$ W m^{-1} K^{-1}, the MPZ, ℓ turns out to be just 2 μm. A simple calculation will show that for bare Nb–Ti the heat required to trigger quench is tiny, just of the order of 10^{-9} J. The problem has, however, been solved by producing composite superconductors with fine filaments embedded in high conducting copper which has a thermal conductivity of about 400 W m^{-1} K^{-1}. This topic has already been discussed in Chap. 6.

7.4.3.2 Quench Voltage and Temperature Rise

A solenoid magnet, in general, is a pure inductance in its normal operation. Part of the winding, however, turns resistive during a quench. This resistive part is shown in Fig. 7.11 as R_Q. During the normal magnet operation the power supply voltage is nearly zero. Small voltage develops during ramp-up (charging) and ramp down (discharging) with opposite polarity. The power supply is turned-off as soon as a quench is detected. Large voltage is generated within the resistive winding which

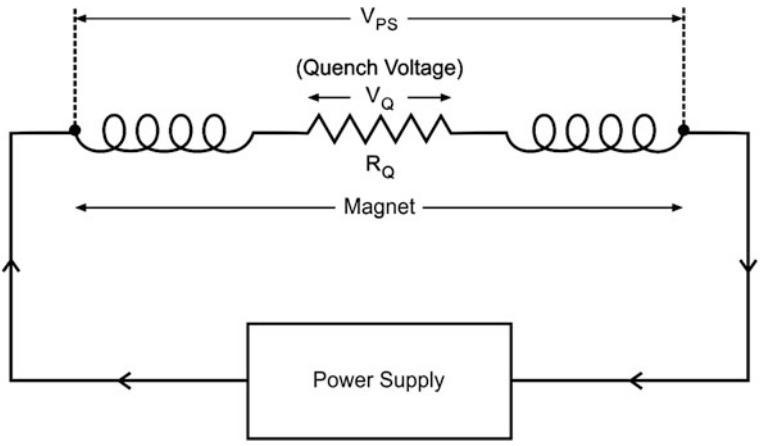

Fig. 7.11 Part of the magnet winding goes resistive (R_Q) and develops huge voltage across this part. Voltage across magnet terminals is restricted to power supply voltage, V_{PS}

can burn insulation and even lead to arcing within the winding. The expression for quench voltage V_Q can be found out from the following equations.

$$V_Q = I R_Q - M \, dI/dt \tag{7.7}$$

and

$$L \, dI/dt = I R_Q \quad (V_{PS} \text{ being zero}) \tag{7.8}$$

where I is the magnet current at the time of quench, R_Q is the resistance of the quenched part, L, the self inductance of the magnet and M, mutual inductance between the resistive part and the rest of the inductance of the magnet.

$$\text{From the two equations } V_Q = I R_Q(1 - M/L) \tag{7.9}$$

V_Q is often of the order of few hundreds or thousands of volts. In the worst scenario, ignoring M, the internal voltage will be

$$V_Q = I R_Q \tag{7.10}$$

With time R_Q will increase and so will M, but the current will fall. The internal voltage will therefore rise to a peak and then fall.

It is extremely important to estimate maximum temperature reached at the point of quench initiation in the winding and keep it restricted, in any case below room temperature. An exact estimate is tedious as the quench process is too fast taking place in a fraction of a second. As the temperature rises the physical properties like resistivity and specific heat keep changing by orders of magnitude. We may follow Maddock and James [16] for the estimation of the maximum temperature and write heat balance equation of the unit volume of the winding.

$$J^2(t) \, dt = C(T) \, dT/\rho(T) \tag{7.11}$$

where $J(t)$, the current density which changes with time t, ρ, electrical resistivity, dt time duration, d, the density and $C(T)$ specific heat at temperature T. All the quantities are averaged over the total winding cross-section. By integrating the above equation we find

$$\int_0^\infty J^2(t) dt = J_0^2 t_d = \int_{4..2}^{T_{MAX}} \frac{dC(T)}{\rho(T)} dT = F(T_{MAX}) \tag{7.12}$$

that the maximum temperature, T_{MAX} is solely dependent on material properties and can thus be worked out by substituting the relevant values in (7.12). J_0 is the initial current density and t_d the decay time of the current after the quench. T_{MAX}

should always be kept under safe limit, in any case well below room temperature. After fixing the maximum upper limit of temperature we can find the decay time of the current and calculate the value of the dump resistance in the protection circuit.

7.4.4 Quench Protection

We have just seen in the previous section that a quench can lead to very serious consequences and destroy a magnet if not protected intelligently. Suppose a magnet with 10 H inductance and running at a current of 200 A quenches in 1 s, it will induce a voltage of 2 kV. The stored energy equal to 0.2, MJ if released in the winding, will burn the winding and can even melt the conductor. Protection circuits are therefore integrated with the magnet so as to dump the energy stored in unquenched part of the winding into an external device and save the magnet. Two types of protection circuits are most popular and used by the scientific community and by the manufacturing companies. These are, one the resistor protection circuit and the other is resistor-diode protection circuit. We briefly discuss them below.

7.4.4.1 Resistor Protection Circuit

This circuit is very simple and cheap. An external low value dump resistance, R_D as shown in Fig. 7.12, is connected across the magnet. The resistance is selected such that the time constant is small for the current to decay and the induced voltage is moderate not exceeding a few kV. Table 7.2 shows the value of time constant, τ ($=L/R_D$) and induced voltage ($=L\ dI_0/dt$) corresponding to the dump resistance of 0.5, 1.0, 10 and 100 Ω for the 7 T magnet discussed in Sect. 7.4.1. The magnet had an inductance of 0.4 H. I_0 is the magnet current at the start of the quench, 210 A in this case. As soon as a quench appears, the power supply detects an increasing

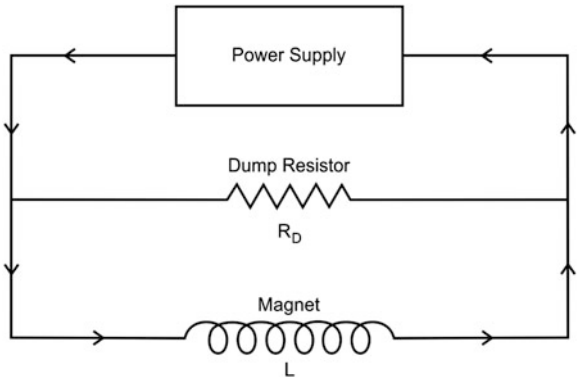

Fig. 7.12 Magnet quench protection by dump resistor, R_D

Table 7.2 Induced voltage corresponding to dump resistance value

Dump resistor R_D (Ω)	Time constant τ (s)	Induced voltage V (volts)
0.5	0.8	105
1.0	0.4	210
10	0.04	2,100
100	0.004	21,000

voltage and switches off automatically. The stored energy is rapidly dumped into R_D according to

$$I = I_0 e^{-(R_D/L)t} = I_0 e^{-(1/\tau)t} \tag{7.13}$$

where t is the time and τ, the time constant. The dump resistor value is kept small as dictated by the requirement of low T_{MAX} and low maximum voltage V_{MAX}, limited to Ohmic voltage across R_D. There is, however, one drawback with the use of resistor that during the ramp-up and ramp-down of the current, the induced voltage drives a current through the dump resistor dissipating heat. This heat will evaporate liquid helium and at high ramp rates can lead to dangerous pressure build-up in the cryostat if the resistor is kept under LHe-bath. As an example, suppose we charge our magnet of 0.4 H inductance and having 0.5 Ω dump resistance across it to 210 A in 1 min, the induced voltage will be 1.4 V. A current of 2.8 A will flow through the resistor dissipating 3.92 W energy. This energy, if released into the LHe-bath will evaporate 5 l/h liquid helium. If the magnet is to be ramped repeatedly this dissipation will add up to very high value and will evaporate large amount of liquid helium. On the other hand, if the same magnet is charged to full current in 10 min the dissipation will be as low as 0.04 W and will evaporate just 52 ml of LHe per hour. To prevent this dissipation from entering the LHe-bath, the dump resistor should be mounted on a radiation baffle in vapour phase. This arrangement assumes greater importance while dealing with large magnets dumping huge energy into the LHe-bath during a quench.

When a magnet is wound in multi-sections, each section is protected against quench by incorporating separate dump resistance across each section. The total stored energy of the magnet is thus divided amongst the sections. In the event of any mishap only the section affected will be damaged.

7.4.4.2 Diode-Resistance Protection Circuit

A better alternative for quench protection is the diode-resistance technique which prevents current flow through the resistor under the influence of induced voltage during ramping up and ramping down. As shown in Fig. 7.13, a set of special diodes is connected in series with the dump resistor. These diodes should be highly reliable, able to function at 4.2 K and sustain current during quench. The number of diodes in the circuit should be chosen such that the forward conducting voltage of the diodes is

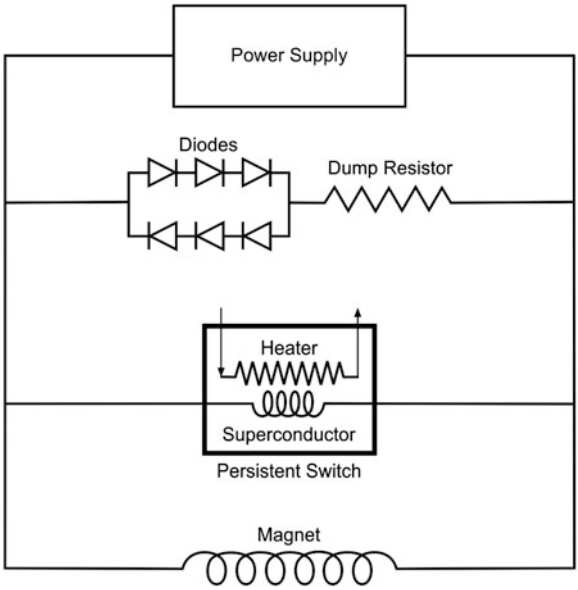

Fig. 7.13 The schematic of a diode-resistor quench protection system for a superconducting magnet. A persistent switch is also shown and connected across the magnet

of the order of few volts. They should not switch on and allow the current to flow through the resistor due to the voltage developed during ramping up and ramping down. Since we need both polarities during ramping we use two sets of back to back diodes in an arrangement shown in Fig. 7.13. This arrangement enables the current in either direction during a quench. At the initiation of quench, the voltages starts rising until the diodes 'switch on' allowing the current to flow through the resistor. The peak voltage is then reached in the resistor. Since in normal operation no current flows through the circuit, this protection system can as well be mounted in LHe-bath. This does away with the need of heavy current leads dumping heat into the bath. Helium evaporation is thus drastically curtailed. In the case of very large magnets we have to have a re-look if the protection system, with or without diodes, should at all be mounted in LHe-bath. During the quench the energy dissipated may cause excessive helium vapour built-up to dangerous level. External dump resistors may be a better option for the protection of huge magnets used in accelerators and fusion reactors. This will be discussed in the next two chapters.

7.4.5 The Persistent Switch

Shown in Fig. 7.13 is also a persistent switch used to run the magnet in persistent mode at a fixed field with power supply switched-off. The switch is connected in parallel with the magnet. The switch has a small non-inductive (bifilar) superconducting winding of 10–100 Ω room temperature resistance and a heater wound over

it. The switch is encased and impregnated with epoxy. To have the superconducting wire of manageable length the wire has a Cu–Ni resistive matrix. During the start-up of the magnet, the heater is 'switched-on' turning the persistent switch normal. The resistance of the switch becomes much higher than the magnet resistance such that the current flows through the magnet and not through the persistent switch. As the current is ramped up the voltage $V = Ir + L\,\mathrm{d}I/\mathrm{d}t$ is seen increasing. Here the first term is the voltage drop across lead resistance 'r' and the second term is induced voltage due to the charging of the magnet. After the required field is achieved, the heater current is 'turned-off'. It is necessary to note down this current. After a pause of 10–20 s the current from the power supply to magnet is reduced to zero. As current through the leads decreases, current through the switch increases to the magnet current level. The current now flows through the magnet in a close-loop and the magnet runs in persistent mode. In NMR and MRI magnets the current leads are de-mountable and are removed once the magnet is put in persistent mode.

A reverse procedure is followed while de-energizing the magnet. Power supply is 'turned-on' and the current raised to the value, at which the magnet was put in persistent mode. The switch heater is now turned-on and the main current is ramped down to the new value as per the new desired field. The switch can be 'turned-off' again to put the magnet in persistent mode. An auxiliary 50 mA power supply is usually in-built in the main power supply for the operation of the persistent switch.

The fabrication of a persistent switch is straight forward and simple but the functioning of the switch strongly depends upon quality of the superconducting joints. Ideally, the joints should have zero resistance. In fact, the jointing technique is a top guarded secret of the manufacturers. The usual steps involved are to etch away the copper cladding of the MF wire, de-oxidize the filaments of the two terminals and twist them. Twisted terminals can be encased in a Nb–Ti sleeve and squeezed under high pressure. This sleeve can be electron-beam welded along the length. There are many variants of this procedure followed by individual laboratories and the commercial establishments. Jointing is more tricky in case of brittle Nb_3Sn and HTS magnets as joints need controlled post heat treatments.

The field does decay with time but quite slowly depending upon the inductance, the design of the switch and the number and quality of the joints. A stability of 10 ppm/h is attained quite comfortably. For high resolution NMR spectroscopy applications, the field stability has to be improved to 0.1 ppm/h and even better.

7.4.6 Training of the Magnet

Training of the magnet is an important part of the magnet operation. Commercial magnets are trained at the factory site before being shipped and need no further training. More often than not, a magnet quenches at a current much below its designed value in the virgin run. The problem is fixed through 'training' the magnet. The specific heat of the superconductor at 4.2 K is small, of the order of 10^{-4} J/g/K and therefore, any tiny thermo-mechanical disturbance in the magnet

can generate heat and form a hot spot which might drive the temperature of the superconductor beyond its T_c. If this hot spot does not subside and propagates, it can lead to quench. Further, a superconducting magnet is a complex composite of several materials like the metallic conductor, the former, inter layer insulation and epoxy used for impregnation. Their thermal contraction coefficients are widely apart. During cool down there is a mismatch in thermal contraction and large stresses are frozen-in. Fracture could occur when large Lorentz forces are built up. Cracks in the epoxy can release strain energy sufficient to cause quench.

Once the strain energy is released, the quench will occur during re-energization at the next level of strain and the magnet can be charged to higher current value. Similarly, the winding adjusts itself against micro movements of the conductor during successive energizations. Experimentally, in the first run of the magnet built in the laboratory, one sweeps the current at low rate to a small value say 10 A/min, stays for a few minute at this level, ramp-down the current to zero. Next time charge the magnet to higher current and ramp-down to zero. This way in a finite number of steps, one goes to the highest designed current. In several of our magnets we did not observe the quench of the magnet during training phase. This must have been due to a perfect winding and good impregnation. Figure 7.14 is a typical training curve of a magnet where the current was ramped-up and ramped-down to a smaller current in steps without inducing quench.

We built many 7 and 8 T magnets in 1970s using many types of impregnating materials like silicon grease, bees wax and epoxy. We have preferred vacuum impregnation route in some and wet winding in others. Both performed admirably well. We found wet-winding, using wax as well as epoxy to be a superior technique. Wet-winding ensures impregnation between each layer and each turn, even though it is a bit messy process. Other advantage is that one can use a filler material with epoxy or wax to reduce the mis-match of the thermal contraction coefficients of the constituents. Filler is not practical in vacuum impregnation technique as the

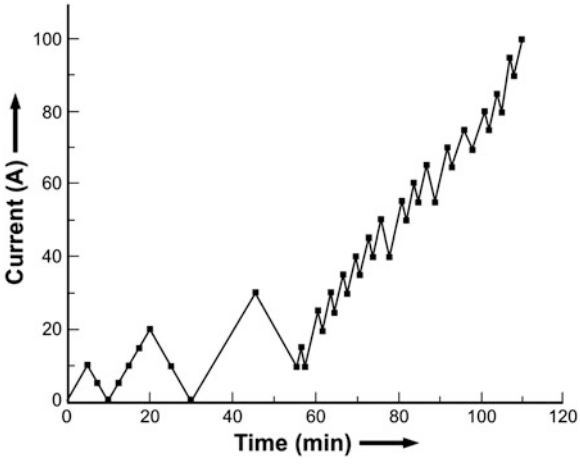

Fig. 7.14 Ramping-up and ramping-down the current in steps during 'training' of a magnet [15]

material has to have low viscosity and has to flow through fine channels. We got excellent results using wet-winding technique using stycast (2,850 FT from Emerson and Cuming) mixed with 20 % Al_2O_3 powder in our cryo-free magnet. As mentioned earlier in many magnets we used fiber glass cloth as the inter-layer which allows free flow of impregnating material during vacuum impregnation process.

7.5 Magnet Power Supply

The superconducting magnet power supply has many features which are unique and quite distinct from the ordinary dc power supplies. Under normal operation it supplies power at low voltage and high current to a high inductance and almost zero resistance load but the magnet can go from pure inductive to pure resistive state during a quench. The power supply detects the quench and switches-off automatically. Circuit design allows variable sweep rates (A/min) for ramping-up and ramping-down the current in a step in the magnet. Four quadrant output capability permits smooth and continuous current reversal through zero current and smooth magnetic field reversal. The power supply can be programmed to sweep magnet current at predetermined different rates at different current levels without user intervention. The voltage limit can be adjusted which in turn puts a limit upon the sweep rate. The supply senses the voltage directly across the magnet bypassing the current leads.

It also has an auxiliary circuit to supply current (0–100 mA) to the heater of the persistent switch. Some supplies also have provision of bi-polarity to supply current in either direction to reverse the direction of the magnetic field. Supplies have computer compatibility using RS 232 or IEEE interface. The power supply has many in-built safety features. It ramps down the current automatically in the event of the detection of power loss and a temperature rise. There are safety interlocks for persistent switch enable/disable and for changing important magnet parameters and limits.

Most power supplies these days are of ‘switching mode’ type which are light in weight and occupy less space. They run in constant current mode instead of constant voltage mode. Power supplies based on linear topology permits operation with less electrical noise and low drifts than switch-mode superconducting magnet power supplies. For high field stability, the current drift at static field should be extremely low for which power supplies based on linear topology are superior. They generate smooth field that is nearly free from offending electromagnetic signatures. Clean field background allows greater resolution in many precision measurements. Modern supplies have firmware module which enables the supply to remember the current at which the magnet was put in persistent mode. This eliminates human error related to the opening of the switch at a wrong current value.

The block diagram of a superconducting magnet power supply system which consists of a switching mode power supply and a programmer built at our Centre (IUAC) [17] several years ago is shown in Fig. 7.15. The programmer consists of a controlled ramp generator and a feedback loop to control power supply. Controlled ramp generator generates desired control signal ramps in the form of straight lines. Controlled loop first generates an error corresponding to current nonlinearity by comparing magnet current with the desired ramp function. This error is then compared with the voltage feedback to compensate for current ramp nonlinearity and voltage drops in the leads. PI type control loop has been developed to improve transient stability performance of the system. The programmer allows a ramp rate between 0 and 10 A/s and an automatic ramp down of magnet current in case of quench. A large rectifier provided at the back of the supply limits the high voltages generated during the magnet quench. These power supplies have been used at the Centre for more than a decade without trouble.

7.6 High Homogeneity Field

We observed in Fig. 7.7 that the field decreases along the magnet axis as we move along the Z-direction away from the centre. The typical field homogeneity obtainable through the judicious selection of the parameters α and β, is limited to about 1 in 10^3 in 10 mm DSV. This homogeneity is, however, quite inadequate for a variety of applications. In principle, field homogeneity can be improved by lowering the peak field at the centre of the magnet by missing certain number of turns in the middle part of the magnet or by adding extra coils at the two ends to enhance the field on either side of the centre. Use of these compensating coils can raise the homogeneity to 10^{-5}–10^{-6} level. NMR magnets need still higher homogeneity of the order of 10^{-9} which is provided by a set of a large number of superconducting 'shim coils' to compensate higher order field expansion terms. We will discuss them in the context of the magnets used in NMR spectrometer in Chap. 10.

Before we discuss the compensating coils to improve the field homogeneity, let us find how the field varies along the axis. To calculate field at point S, a distance Z (Fig. 7.16) away from the centre along the axis. We can make use of the (7.1) and (7.2) and divide the solenoid magnet into two parts as shown in Fig. 7.16, each part being half of a solenoid. The field at the end of the solenoid magnet can be taken as half of the field at the centre. The field at the point S can thus be written as:

$$B_z = \frac{1}{2} J \lambda a_1 [F(\alpha \cdot \beta_1) + F(\alpha \cdot \beta_2)] \tag{7.14}$$

where $\alpha = a_2/a_1$, $\beta_1 = (\ell - Z)/a_1$ and $\beta_2 = (\ell + Z)/a_1$. It is to be noted that β_1 becomes negative for $Z > \ell$, for points outside the end point of the magnet, $F(\alpha, \beta_1)$ should therefore be taken as $F(\alpha, -\beta_1)$, or $= -F(\alpha, \beta_1)$. Following Montgomery [10] the

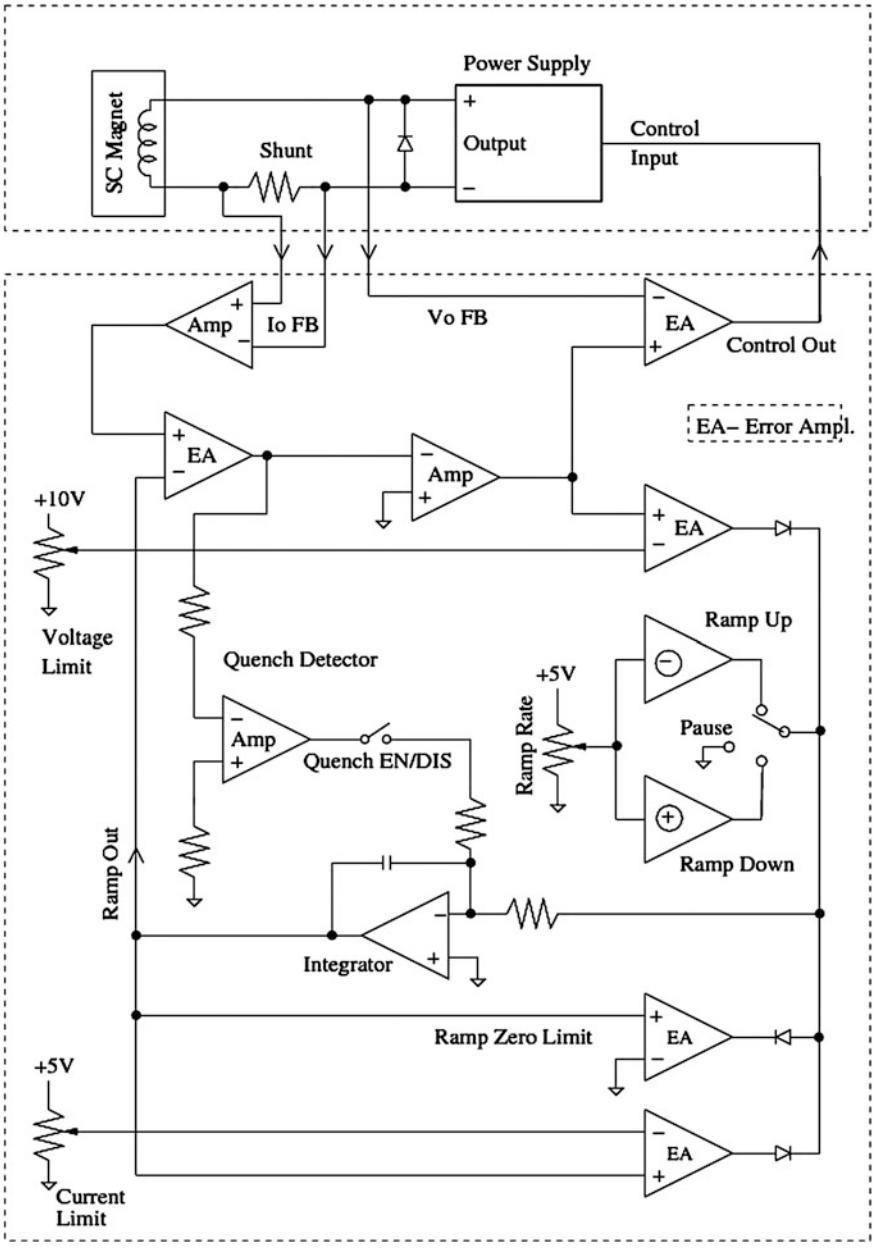

Fig. 7.15 The block diagram of a superconducting magnet power supply system consisting of a switching mode power supply (6 V, 100 A) and the programmer [17] (*Courtesy* Rajesh Kumar, IUAC Delhi)

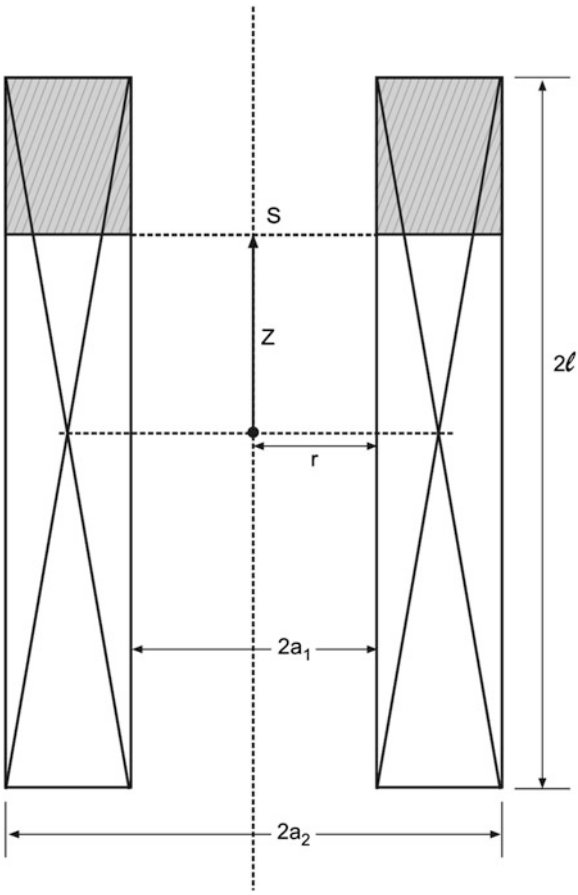

Fig. 7.16 To find field at a distance Z from the centre, magnet is divided into two parts each one-half of a solenoid. β for the two solenoids will now be $(\ell + Z)/a_1$ and $(\ell - Z)/a_1$

axial and radial components of the axial field in a centrally symmetric solenoid can be written as the expansion series as:

$$B_Z(Z,0) = B_0\left[1 + E_2\left(\frac{Z}{a_1}\right)^2 + E_4\left(\frac{Z}{a_1}\right)^4 + E_6\left(\frac{Z}{a_1}\right)^6 + \cdots\right] \tag{7.15}$$

$$B_Z(0,r) = B_0\left[1 - \frac{1}{2}E_2\left(\frac{r}{a_1}\right)^2 + \frac{3}{8}E_4\left(\frac{r}{a_1}\right)^4 - \frac{5}{16}E_6\left(\frac{r}{a_1}\right)^6 + \cdots\right] \tag{7.16}$$

where the error coefficients E_n are given from the standard formula for the coefficients in a Taylor series:

$$E_{2n} = \frac{1}{B_0}\left(\frac{1}{(2n)!}\right)\frac{d^{2n}B_Z(Z,0)}{d_Z^{2n}} \quad Z = 0 \tag{7.17}$$

The values of these coefficients can be determined by taking the derivative of the field (7.14) with respect to Z, that is, along the axis and evaluating them at $Z = 0$. First few E_{2n} dominant terms have been given by Montgomery [10] (Table 8.2, p. 236). It is noticed from (7.15) and (7.16) that near the centre where r/a_1 is small, the E_2 term dominates and the deviation of the field in the radial direction is only half of that along the axis. For a simple solenoid E_2 term is always negative. The field along the axis decreases but increases in the radial direction until $r = a_1$. It decreases thereafter because of certain boundary conditions.

7.6.1 High Homogeneity Field by Compensated Coils

Field expansion (7.15) and (7.16) indicate very clearly that in a solenoid magnet the inhomogeneity in the axial field along longitudinal and radial directions come from the higher order terms in these equations. To get high homogeneity fields it is therefore imperative to get rid of the successive terms in these equations. Larger the number of terms eliminated, higher is the homogeneity of the field. This can be achieved by subtracting a smaller coil from the main coils so as to cancel higher order terms. These compensating coils operate at the same current level as the main coil. Compensating coils will look like a gap or will appear as a notch in the main winding. The number of terms to be cancelled depend upon the number of variable geometrical parameters chosen for the compensating coil. For example, with one of the variable parameters α and β keeping same for both the coils and varying the other parameter, we can cancel one term, E_2. The magnet will be compensated to fourth order similar to a Helmholtz coil. With two variable parameters α and β one can cancel two terms, E_2 and E_4 compensating the main coil to sixth order. This compensating coil can be incorporated either at the inner winding bore or at the outer winding bore and are referred to as 'inside notch' and 'outside notch' respectively.

The fourth order compensation geometry is shown in Fig. 7.17, which is just a Helmholtz coil. Here the missing coil is the gap in the middle of the main coil. The main coil as also the gap has the same value of $\alpha(\alpha = \alpha_c = a_2/a_1)$ but different values of parameter β. As seen in Fig. 7.17 β for the main coil is ℓ/a_1 while for the correction coil β_c is ℓ_c/a_1. Here the subscript 'c' indicates the parameters for the compensating coil.

For sixth order compensation (E_2 and $E_4 = 0$), both 'inside notch' and 'outside notch' geometry are possible and are shown in Fig. 7.18. Shaded areas are the missing part or the so-called compensation coils. In sixth order (inside notch) again has the same a_1 as for the main coil. The modified field expression for the combined coil can now be written as

$$B_z(Z,0) = J\lambda a_1 \Big[F_0(\alpha,\beta) - Fc(\alpha_c,\beta_c) + \{F_0 E_2(\alpha,\beta) - F_0 E_2(\alpha_c,\beta_c)\}(Z/a_1)^2 + \{F_0 E_4(\alpha,\beta) - F_0 E_4(\alpha_c,\beta_c)\}(Z/a_1)^4 \ldots\Big] \tag{7.18}$$

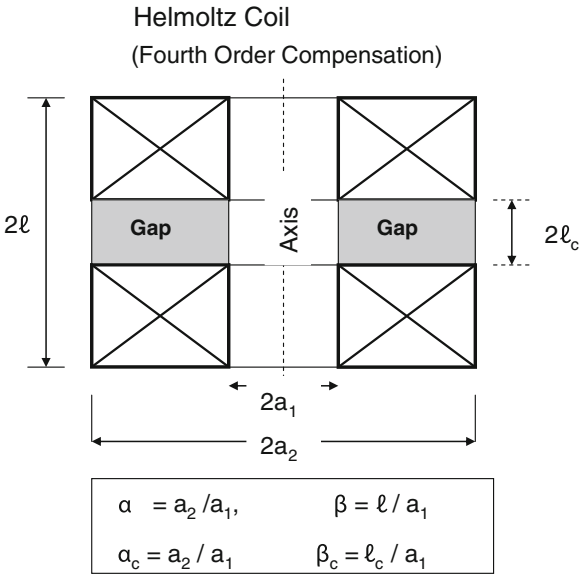

Fig. 7.17 Graphical representation of the fourth order compensation. Note same value of α for the main coil as well as for the compensating coil but different values of β and β_c

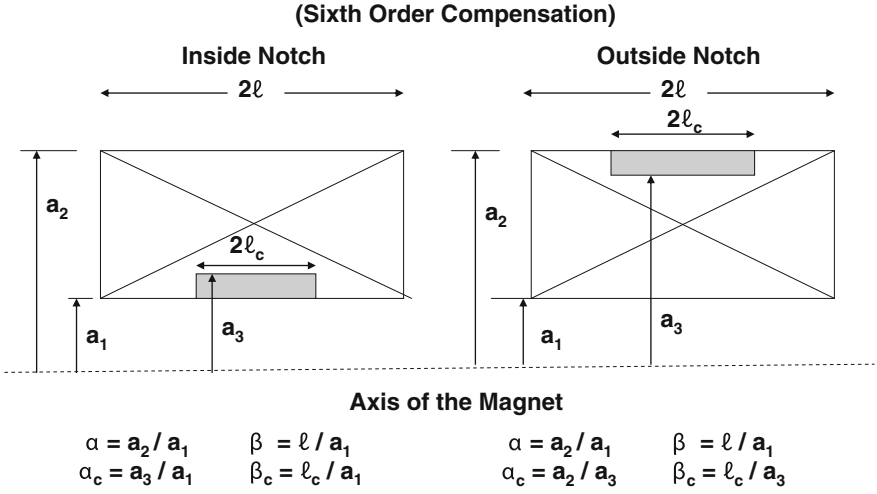

Fig. 7.18 Graphical representation of sixth order compensation, 'inside' (*left*) and 'outside' (*right*). Missing turns are shown shaded. Values of α, β and α_c, β_c have also been written

For fourth order compensation the terms $F_0\, E_2(\alpha, \beta)$ and $F_0\, E_2(\alpha_c, \beta_c)$ are equal and opposite in sign and therefore cancel out. The field uniformity improves. The functions $F\, E_2(\alpha, \beta)$ and $F\, E_4(\alpha, \beta)$ when plotted against β for different values of

α show a peak which means that there are two values of β for each value of the functions $F_0\ E_2(\alpha, \beta)$ and $F_0\ E_2(\alpha_c, \beta_c)$ for the same value of α. The smaller value of β on the left of the peak yields β_c for the small compensating coil. Since the inner diameter of the compensating coil (both fourth order and sixth order, inside notch) is the same as that of the main coil the corresponding length of the compensating coil can be calculated from β_c.

Figure 7.19 shows the contours of constant FE_2 and FE_4 intersecting at two points. Intersection at $\alpha = 3$ and $\beta = 2$ corresponds to the main magnet and the second intersection at $\alpha_c = 1.87$ and $\beta_c = 1.33$ corresponds to the sixth order compensating coil. The cancellation of the first two terms, FE_2 and FE_4 thus leads to much more field homogeneity than the fourth order Helmholtz coil. It is important to control the dimensions of the compensating coils very precisely, within 2 % of the calculated value, homogeneity being extremely sensitive to the errors in choosing the dimensions. This sensitivity is significantly reduced by choosing β much larger than the minimum coil volume criterion. The magnitude of the higher order terms to be cancelled is significantly reduced.

Very useful tables for the design of the compensating coils have been given by Montgomery [10] for fourth order, for sixth order compensation inside notch and outside notch. We made a few Nb–Ti magnets of the sixth order compensation using these tables in early 1970s. One, rather long and low field (2.35 T) solenoid magnet with $\alpha = 1.224$ and $\beta = 3.38$ we built [18] using outside notch gave us an homogeneity of 3×10^{-6} in 10 mm SDV.

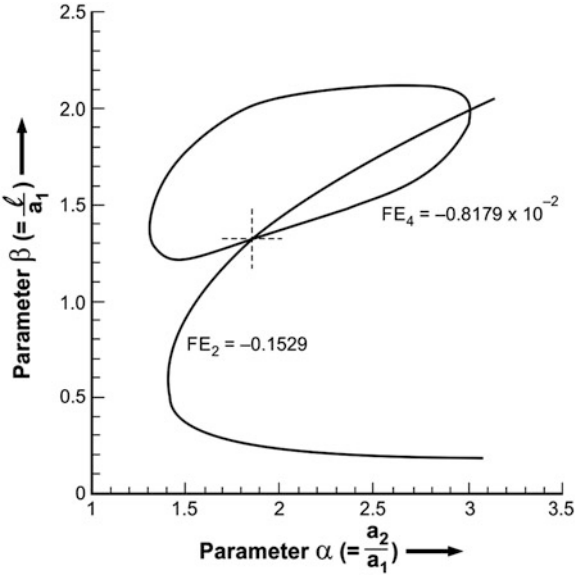

Fig. 7.19 The contours of constant FE_2 and FE_4 intersecting at two points Intersection at $\alpha = 3$ and $\beta = 2$ corresponds to the main magnet and the second intersection at $\alpha_c = 1.87$ and $\beta_c = 1.33$ corresponds to the sixth order compensating coil [10] (*Courtesy* D.B. Montgomery "Solenoid Magnet design")

7.7 Nb_3Sn Magnets

For field production above 9 T and at 4.2 K, our option is limited to the A-15 Nb_3Sn superconductor. With the availability of Nb_3Sn conductors produced by improved techniques and elemental additions (Chap. 6), field higher than 21 T have been produced [19] in 1990s. In general, such high field magnets consist of a number of concentric solenoids. The outermost solenoid is a Nb–Ti coil providing a background field of 8 T. The inner coils are wound using Nb_3Sn, (Nb, Ti)$_3$Sn and (Nb, Ta, Ti)$_3$Sn conductors. First 1 GHz (1,000 MHz) NMR spectrometer (BioSpin) was installed by Bruker in 2009 in France which has a superconducting magnet producing a field of 23.5 T. 930 MHz spectrometers using superconducting magnets are in use for some years at Tsukuba Magnet Laboratory, National High Magnetic Field Laboratory, Florida and many such other places. High field magnet usually produce 20–21 T field using a combination of Nb_3Sn coils and an inner-most coil of high T_c Bi-superconductor. This Bi-2223 coil is now being replaced by superior 2G-RBCO coils. Standard Nb_3Sn magnets going up to 20 T are now manufactured by cryogenic industries and are usually integrated with various measurement systems.

Building Nb_3Sn magnets is quite difficult as compared to Nb–Ti magnets. The main reason being the extreme brittleness of this material. Commercial multifilamentary cryo-stabilized Nb_3Sn wires and cables are by and large available in pre-reacted form, that is, with Nb-filaments in Cu–Sn bronze matrix. The wire is ductile enough to be wound into a coil. The coil is then heat reacted at high temperature under controlled conditions whereby Sn from the matrix diffuses into Nb-filaments to form intermetallic Nb_3Sn. The magnet is then impregnated as usual but extreme care is required to handle the reacted magnet.

7.7.1 Construction Details of an 11 T Magnet

As an example we take-up the construction of an 11 T magnet which we built [20] many years ago as an exercise. The magnet is a combination of an outsert of Nb–Ti coils and an insert of Nb_3Sn coil. The Nb–Ti outsert magnet provides a background field of about 7.2 T and the rest generated by the insert Nb_3Sn coil. The magnet coils were designed as per the standard procedure described in Sect. 7.4. In brief, the magnet had a working bore of 50 mm and a total of three sections. Outer two sections were wound using MF Cu/Nb–Ti wires. The Nb–Ti magnet had a clear bore of 100 mm to accommodate Nb_3Sn coil. It's winding length was 220 mm. All the actual dimensions of all the coils and other magnet parameters [21] have been listed in Table 7.3. We used a Nb–Ti wire of 0.75 mm diameter for winding the inner coil and 0.54 mm for the outer coil of the Nb–Ti outsert. Both the coils were wound one over the other on the same former. The formers for Nb–Ti magnet as well as for Nb_3Sn magnet were made out of SS 304. The cylindrical part of both the formers were uniformly perforated to allow liquid helium to cool the inner parts of

Table 7.3 Parameters of a 11 T superconducting magnet [21] working bore Dia. = 50 mm

Sr. no.	Parameter	Inner most coil (Nb_3Sn)	Outer coil (Nb–Ti)	
			Inner section	Outer section
1	Inner winding dia.	56.6 mm	110.6 mm	148.8 mm
2	Outer winding dia.	100 mm	148.5 mm	180.5 mm
3	Winding length	170 mm	220 mm	220 mm
4	Parameter α	1.766	1.34	1.21
5	Parameter β	3.00	1.99	1.48
6	Parameter $F(\alpha, \beta)$	0.873×10^{-6}	0.36828×10^{-6}	0.21149×10^{-6}
7	Conductor used	Nb_3Sn	Nb–Ti	Nb–Ti
8	Conductor dia.	0.85 mm	0.75 mm	0.54 mm
0	No. of filaments	6,000	54	54
10	No. of layers	20	22	26
11	Total no. of turns	3,863	6,458	10,584
12	Field at 90.5 A	2.395 (T)	Field by Nb–Ti coils 7.315 (T)	
13	Final field with 90.5 A in Nb–Ti coils and 140 A in Nb_3Sn coil		11.03 (T)	
14	Conductor length (approx.)	1 km	2.65 km	5.6 km
15	Interlayer material	Fibre glass cloth		
16	Impregnation (vacuum)	Bees wax		
17	Quench protection	Through dump resistor		

the coil. Similarly, the two end flanges of both the magnets had perforation and also curved radial slots enabling again cooling by liquid helium and taking the end terminals of the coils out. For Nb_3Sn coil we used a bronze-processed 'wind and react' wire of 0.85 mm diameter supplied by Vcuumschmelze, Germany. We had no choice of choosing wire diameters optimized for the same current but had to use the wires available and we could procure.

7.7.2 Winding the Background Nb–Ti Magnet

The winding of the Nb–Ti magnet was carried out as outlined in Sect. 7.4 except that now the magnet was wound in two sections. The inner coil was wound using 0.75 MF Cu/Nb–Ti wire. As Table 7.3 shows a total of about 2.65 km of wire was used and wound in 22 layers and 6,458 turns in all. Fiber glass cloth was used as inter-layer material. The outer section was wound on the inner section using MF Cu/Nb–Ti wire of 0.54 mm diameter. We used about 5.6 km of this wire in 26 layers and 10,584 number of turns. The end terminals of the coils were wrapped over the copper studs which had spiral grooves. Sufficient length of the wires was wrapped and soldered with Pb–Sn solder. This was to make very low resistance joints. Vapour-cooled current leads were taken out to the top plate of the cryostat. The three current terminals at the top plate enabled us to operate the two coils either in series or individually. The magnet was vacuum-impregnated in bees wax following the standard procedure.

7.7.3 Winding the Nb_3Sn Magnet

Winding the Nb_3Sn magnet is rather tricky. This is for several reasons. The first one is that since the wire is finally to be reacted at high temperature, it does not have the usual electrical insulation. The wire is covered with a glass sleeve which is quite fragile. Handling the wire during winding is thus a difficult task. Glass cloth was used as interlayer. The space factor 'λ' in Nb_3Sn coil is smaller than in the case of Nb–Ti coils. As shown in Table 7.3 the magnet had a clear working bore of 50 mm and an inner winding diameter of 56.6 mm. Here again we preferred SS-304 former. The winding length was 170 mm. A bronze processed Cu–Sn/Nb wire of 0.85 mm diameter with glass sleeve cover was used for winding. The wire had 6,000 filaments. In all, we had 20 layers and a total of 3,836 number of turns.

7.7.4 Preparation of Current Terminals

Before carrying out heat treatment, it is essential to fix the coil terminals on to a pair of copper studs without removing the glass sleeves from the wires. Figure 7.20 shows the Nb_3Sn coil before heat treatment (a) and after the heat treatment (b). It is seen clearly from these figures that the wire terminals of the coil have been taken

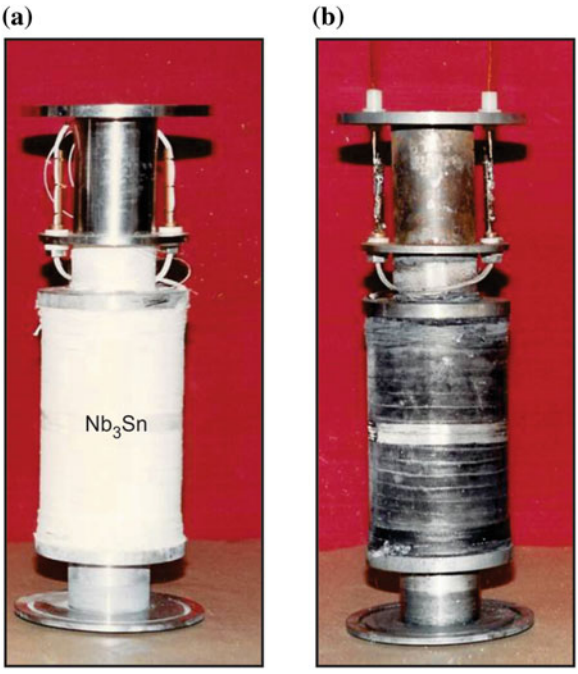

Fig. 7.20 The Nb_3Sn coil before heat treatment (**a**) and after heat treatment (**b**). Note how the coil terminals have been taken out through the metallic flanges using ceramic spacers to prevent electrical shorts [21] (*Photo courtesy* NPL Delhi)

out through the ceramic bushes fixed in the metal flanges to prevent electrical contact. The two long copper studs have a central hole and half circular cross-sections. The coil terminals are tied with the help of a copper wire on to these two studs at several places. The precaution to be taken here is that the glass sleeve should be in place along the entire length of the wire. At no place the superconducting wire should come in contact with the copper studs. If by chance it happens the Sn from the bronze wire will diffuse into copper studs during the heat treatment and stoichiometric Nb_3Sn will not form, making the magnet unusable.

7.7.5 Heat Treatment and Impregnation

Now comes the most critical phase of the magnet fabrication. The pure Nb-filaments embedded in Cu–Sn bronze have to be converted into Nb_3Sn filaments. Before going in for heat treatment of the magnet we kept the magnet under running water to get rid of starch coated on glass sleeve and glass cloth. Earlier through some preliminary study on the heat treatment of the short sample of the bronze wire we found the glass sleeve to be charred and covered with thick layer of carbon. Significant amount of starch was washed out from the magnet winding by the process we followed. As discussed in detail in Chap. 6, a two-step heat treatment is advisable to get high critical current density in the wire. A long heat treatment at comparatively lower temperature enables the formation of small size grains in the Nb_3Sn compound which is a prerequisite for all A-15 superconductors to have high J_c. This treatment should be followed by a second heat treatment for a shorter period but at higher temperature to improve stoichiometry of the Nb_3Sn which in turn raises the upper critical magnetic field B_{c2} and thus J_c.

Another important step in the heat reaction is that there should be no trace of oxygen in the reactor. The heat treatment must be carried out either in vacuum or under inert gas atmosphere. For all our Nb_3Sn magnets we carried out heat treatment under flowing high purity argon gas. The reactor chamber was thoroughly pumped and flushed several times with Ar-gas after the magnet was loaded into the reactor. The magnet was kept at a temperature of 120 °C for many hours to get rid of moisture. Out of a few options of heat treatment schedules given by the supplier of the wire we chose a two step process. The magnet was kept at 570 °C for 120 h followed by another heat treatment of keeping the magnet at 700 °C for 80 h after which the magnet was furnace cooled. The real challenge comes at this stage, how to handle the brittle magnet right from the stage of taking it out of the reactor, making current contacts and carrying out impregnation. To make electrical contacts of the coil terminals with the copper studs, the glass sleeve is very carefully removed and the reacted wire is cleaned. These bare wire terminals are now soldered with the Cu-studs using (Pb–Sn) solder along the full length. The next step is the impregnation of the magnet using either bees wax or the epoxy in a way similar to the Nb–Ti magnets. After the impregnation handling of the magnet becomes easier.

7.7.6 Assembly of Magnet Coils and Operation

The Nb_3Sn magnet is nested inside the Nb–Ti magnet and rigidly fixed in position. The combined magnet is then suspended from the support structure consisting of radiation baffles, liquid helium level sensor, LHe-fill line and G-10 support rods. A ll the three sections of the magnet were protected against quench independently by separate dump resistors which were mounted in the vapour phase. Separate vapour-cooled current leads were taken out from the two magnets such that they can be energized independently as well as jointly by making series connection outside the cryostat at the top plate. The combined magnet is shown in Fig. 7.21 and the whole magnet assembly along with the support system in Fig. 7.22.

Standard procedure for the operation of the magnet can now be followed to cool down the magnet system to 4.2 K and energize. Two power supplies were used because of the mismatch of the currents in the two magnets. The Nb–Ti magnet produced a field of 7.315 T at a current of 90.5 A, whereas the Nb_3Sn magnet generated an additional field of 3.715 T at a current value of 140 A. A total field

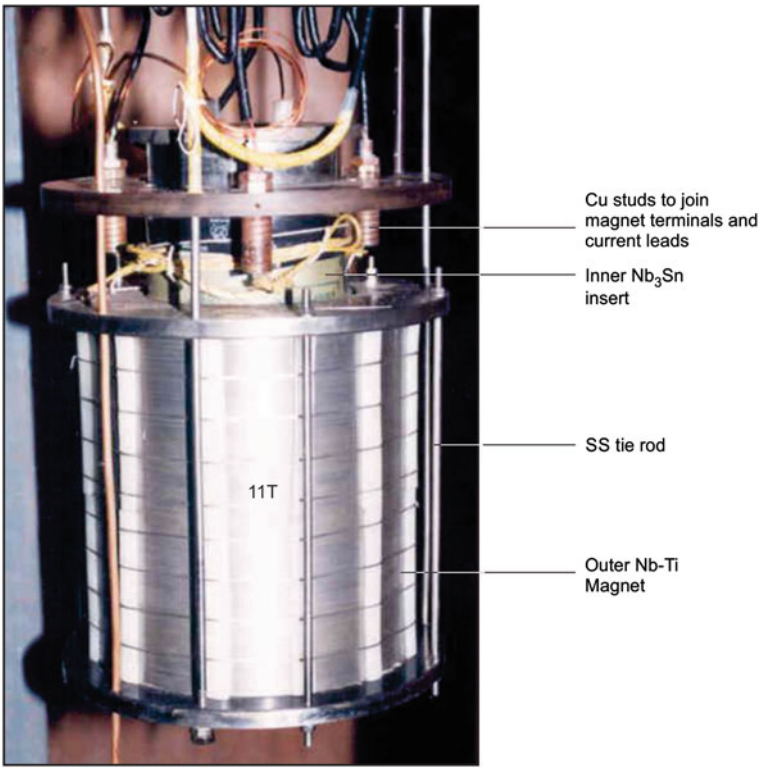

Fig. 7.21 The 11 T Nb–Ti/Nb_3Sn magnet made in author's laboratory in early 1990. The outer coil seen is the Nb–Ti magnet with tie rods. Liquid helium fill-line and level meter too are seen on the *left*. Nb_3Sn insert coil is in the *centre* [21] (*Photo courtesy* NPL Delhi)

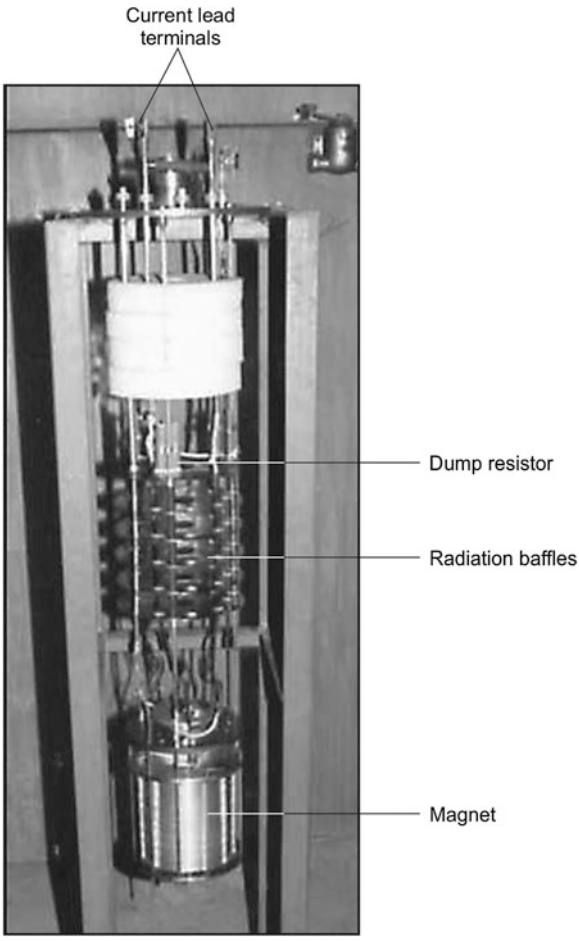

Fig. 7.22 The Nb–Ti/Nb_3Sn magnet along with the support system [21] (Photo courtesy NPL Delhi)

of 11 T is thus achieved as per the objective of this magnet. During the training, we ramped-up and ramped-down the field in steps of 10 A, no quench occurred in any of the coils. The *I–B* profiles of the Nb–Ti magnet, the Nb_3Sn magnet and the two in combination are plotted in Fig. 7.23.

7.8 Intense Field Magnets

7.8.1 A 21.1 T Superconducting Magnet Built by NIMS

Great strides have been made in the production of fields of the order of 20 T and above using the combinations of two metallic superconductors, namely the Nb–Ti and the A-15 Nb_3Sn. Having built world's first highest field 17.5 T all

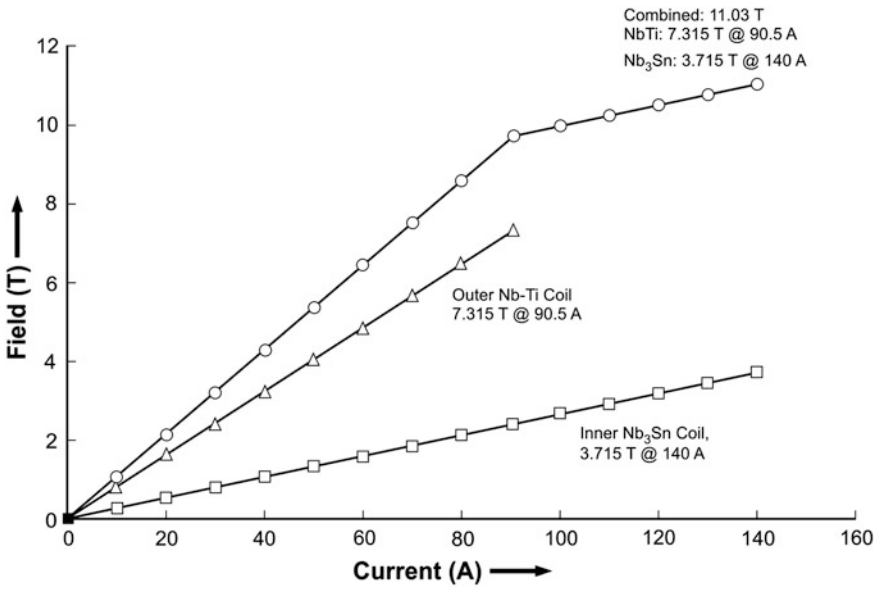

Fig. 7.23 The field versus current relationship for the Nb–Ti (*middle curve*) and Nb_3Sn magnet (*lower curve*). The *I-B* profile of the combined magnet is the *top curve* producing a field of 11 T [21]

superconducting magnet [22], the NRIM, Japan now called NIMS (National Institute of Material Science), has been a forerunner in enhancing this field steadily to higher than 21 T. The 17.5 T magnet was built using Nb_3Sn and an insert coil of V_3Ga developed by NRIM by diffusion process. With the improvement in J_c of Nb_3Sn through elemental additions, V_3Ga has been pushed to the background by Nb_3Sn which is comparatively cheaper also. The field was increased to 21.1 T [23] by NIMS in 1994 by using coils of Nb–Ti, (Nb, Ti)$_3$Sn and (Nb, Ta, Ti)$_3$Sn conductors. This magnet was an improvement over the earlier magnet built by NIMS [24] producing a field of 20.33 T in a clear bore of 44 mm. The new magnet replaced the inner most coil by a coil which was wound using (Nb, Ta, Ti)$_3$Sn conductor and following a 'wind and react process'. This conductor had much lower copper ratio of 0.48 in place of the earlier conductor which had a ratio of 0.8. This meant a much higher current density. Yet another innovation carried out was the removal of the SS former of this inner most coil. This made available a larger working bore of 50 mm and also prevented high stress between the former and the coil.

The new (Nb, Ta, Ti)$_3$Sn conductor was developed at NIMS wherein 0.5 at.% Ta has been added to Nb and 0.6 at.% Ti to the Cu–Sn matrix. These composite cores are bundled together in a Cu–Sn bronze tube and processed. These processed MF strands are stacked together in a Cu-tube, for stability, with a Nb diffusion barrier and reduced to desired size of the conductor. The outer-1 coil was wound using a Cu-stabilized rectangular cable having 11 twisted strands of (Nb, Ti)$_3$Sn and the

Table 7.4 Parameters of the 21 T Magnet built in 1994 at NIMS (data compiled from [23] with permission from Elsevier)

Magnet coil	Inner most $(Nb, Ta, Ti)_3Sn$	Middle $(Nb, Ti)_3Sn$	Outer-1 $(Nb, Ti)_3Sn$	Outer-2 (Nb–Ti)
Inner coil dia.	50 mm	180 mm	380 mm	801 mm
Outer coil dia.	151.2 mm	291.8 mm	725.6 mm	1175.8 mm
Coil length	220.3 mm	463.5 mm	1,230 mm	1,293.6 mm
Coil form	solenoid	31 double pancakes	40 double pancakes	41 double pancakes
Total no. of turns	1,760	1,364	1,520	2,296
Conductor dimensions	2.42 × 2.0 mm	6.0 × 2.0 mm	13.4 × 8.15 mm 11 strand ract. cable	13.8 × 6.0 mm 19 strand ract. cable
Process	Bronze process wind and react	Bronze process wind and react	Bronze process react and wind	Normal commercial process
Operating current	350 A	910 A	4,717 A	4,717 A
Field produced	2.5 T	3.6 T	Total (Both Coils) 15 T	
Total field	21.1 T @ 4.2 K			

outermost coil using a Cu-stabilized rectangular conductor of 19 twisted strands of Nb–Ti. The complete parameters of the magnet are given in Table 7.4.

The total magnet system is housed in a cryostat with two separate chambers in vacuum. The outer chamber houses the two outer coils and the inner chamber remaining two inner coils. The two outer coils were connected in series and jointly produced a field of 15 T. The middle coil generated an additional field of 3.6 T at an operating current of 350 A. The inner-most coil was run on an independent power supply and added another 2.5 T. The operating temperature was maintained at 1.8 K. The total field produced was 21.16 T, the highest ever reported using only the metallic superconductors, that is, without the use of a HTS insert coil. The complicated nature and the shear size of such magnet can be gauged from Fig. 7.24 where the assembly of a 21 T magnet [25] is going on at TML (NIMS). This particular magnet produced a field of 21.5 T field at 1.8 K in a clear bore of 61 mm good enough to accommodate an inner HTS coil to produce still higher fields.

7.8.2 Ultra High Field Superconducting Magnets

The production of very high or ultra high magnetic field is limited not so much by cost as by the stringent requirement of the superconducting material to carry high current in presence of intense magnetic field and to withstand very large electromagnetic forces (=BJR). Low Temperature Superconductors (LTS) based

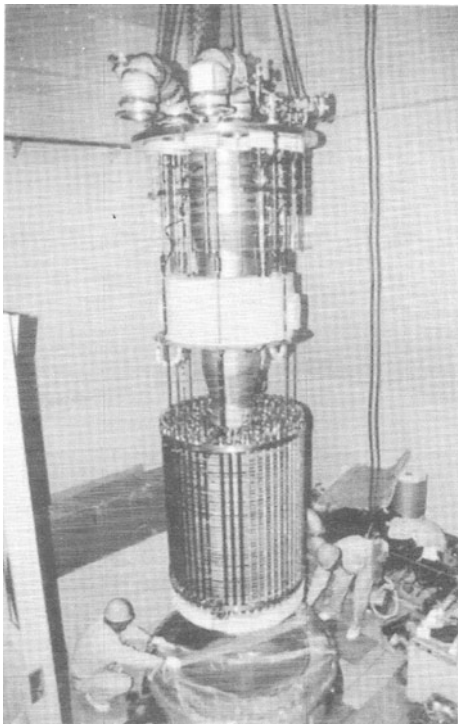

Fig. 7.24 The on-going assembly of the outer coils of a 21.5 T superconducting magnet at the Tsukuba Magnet Laboratory, Japan [25] (With permission from Elsevier)

magnets discussed in the last section seem to have saturated once at 21.5 T even when we operate them at superfluid helium temperature (1.8 K). The only hope to raise further this limit appears to be the HTS conductors. Even though, the dream of producing high magnetic field at 77 K has not been realized so far, yet these materials have shown promise in pushing the field limit well beyond 21.5 T, only if HTS magnets are operated at 4.2 K, their B_{c2} being very high. Their critical current values are very high at large field when operated at such low temperatures. One problem peculiar to HTS is the strong anisotropy of J_c with magnetic field direction. The current has to flow parallel to the wider surface of the tape conductor and the magnetic field should be parallel to the c-axis. Since the magnetic lines bend at the edge of the magnet, the field no longer remains parallel to the c-axis. The critical current density of the conductor decreases with angle of field orientation. J_c at the magnet-end and not at the mid-plane should therefore be found out after the dimensions of the coils are frozen. The conductor intended to be used is to be thoroughly characterized for its J_c with respect to field orientation. This is not the problem with LTS magnets. The next step is to produce these superconductors sufficiently flexible and with high stress tolerance through cladding with high strength material. Technology to produce HTS in long length needs to be upgraded.

The driving force to produce ultra high magnetic field using superconducting magnets has come from researchers from solid state physics, chemistry and the life

sciences. Availability of such intense magnetic field will lead to new phenomena, hitherto undiscovered in a variety of solids and also open up possibility of building ultra high field NMR spectrometers with unprecedented resolution. It will then be possible to study extremely complex molecular structure of proteins and similar species. The strategy to attain high field has been to generate maximum possible field by the suitable combination of the Nb–Ti and Nb_3Sn coils and using an inner most HTS coil as an insert. For highest field the magnet is operated at 1.8 K. Until recently, BSCCO 2212 and 2223 have been the favorite materials for winding the magnet coils. But during last few years REBCO coated superconductors with superior performance have been developed and marketed by a number of companies in USA and Japan. Record high field have been produced using these combinations. Below we discuss very briefly the most notable developments that have taken place in past few years.

7.8.3 A 24 T Magnet Using GdBCO Insert Coil

A team led by S. Matsumoto at TML, Japan had produced a record breaking field of 24 T in 2011. The details of this, all superconducting 4.2 K magnet, have been published recently [26]. The inner most coil has been wound using GdBCO thin film wire produced by Fujikura Ltd. Japan and vacuum-impregnated in wax. The beauty of the magnet is that it operates at 4.2 K instead of 1.8 K which is so much simpler to handle than a superfluid. The coil generates a field of 6.8 T at a current level of 321 A and a an electromagnetic force BJR of 408 MPa. The coil has a clear bore of 40 mm and is nested in a combination magnet of Nb–Ti and Nb_3Sn generating together a background field of 17.2 T. Some of the parameters of this magnet system are given in Table 7.5.

Table 7.5 Some parameters of the 24 T magnet coils [26] (With permission from Shinji Matsumoto and IOP)

Coil	Unit	Inner most coil
Conductor (tape)		(Gd–Ba–Cu–O)
Coil inner dia.	mm	50.27
Coil outer dia.	mm	112.80
Coil height	mm	88.33
Conductor dimensions (w × t)	mm × mm	5.00 × 0.15
Total no. of layers		124
Total no. of turns		2,010
Total conductor length	m	515
Operating current	A	360
Central field by the inner coil	T	7.6
Background field by Nb–Ti and Nb_3Sn coils	T	17.2
Total central field	T	24.8

As mentioned above a background field of 17.2 T is provided by a combination of Nb–T and Nb_3Sn outserts. The middle coil is a Nb_3Sn coil with 135.2 mm inner dia., 318.4 mm outer dia. and has a height of 440 mm. It produces a field of 8.2 T at an operating current of 241.1 A. The outermost coil is a Nb–Ti coil with an inner dia. of 330.3 mm, outer dia. 516.8 mm and a height of 710 mm. It produces a field of 9.0 T at an operating current of 241.1 A. The highest central field produced thus turns out to be 24. 8 T @ 4.2 K.

7.8.4 Recent High Field Magnet Developments at FSU

7.8.4.1 A 26.8 T YBCO Insert Coil

Yet another important development towards the goal of achieving 30 T field by using HTS inserts took place at FSU in 2007. The NHMFL in collaboration with SuperPower produced a coil using coated YBCO tape conductor. The coil produced a record field of 7.8 T in a background field of 19 T generated by a 20 MW, 20 mm bore resistive magnet [27] and yielded a combined field of 26.8 T. The coil had a clear bore of only 9.5 mm but it did establish the possibility of generating field in excess of 30 T HTS insert coil operated at liquid helium temperature, 4.2 K.

7.8.4.2 A Record Field of 32 T

FSU has already designed a whole superconducting magnet using inner insert coils of REBCO coated superconductor to produce a record field of 32 T in a 32 mm bore. It has already tested a REBCO insert coil producing a total field of 32 T [4, 5] in a 32 mm bore in a background field of 20 T generated by a resistive coil. This happens to be a world record of field produced by a combination of superconducting and resistive magnets at the present time. This is a landmark development and deserves to be discussed a bit in detail. These efforts were aimed at technology demonstration and resolve problems related to conductor behaviour under conditions of high field and high mechanical stresses, its I_c-B behaviour vis-à-vis field orientation and strain effect, the quench protection, the jointing of the conductor crucial to the stability of field required in NMR type applications and so on.

The first prototype of the 32 T magnet [28] has already been fabricated and tested in a back ground field 15.14 T produced by a set of Nb–Ti and Nb_3Sn LTS coils. The central REBCO coils generated a field of 17.4 T. The photograph of the REBCO coils with its support structure is shown in Fig. 7.25. Important parameters of the 32 T magnet are given in Table 7.6.

The paper [28] does not identify the rare earth 123 compound used for inner coils. It can be conjectured that various options of rare earth-123 compounds might have been evaluated. Two REBCO HTS coils nested one inside the other have been used. The inner HTS coil has an inner dia. 40 mm and outer dia. 140 mm and

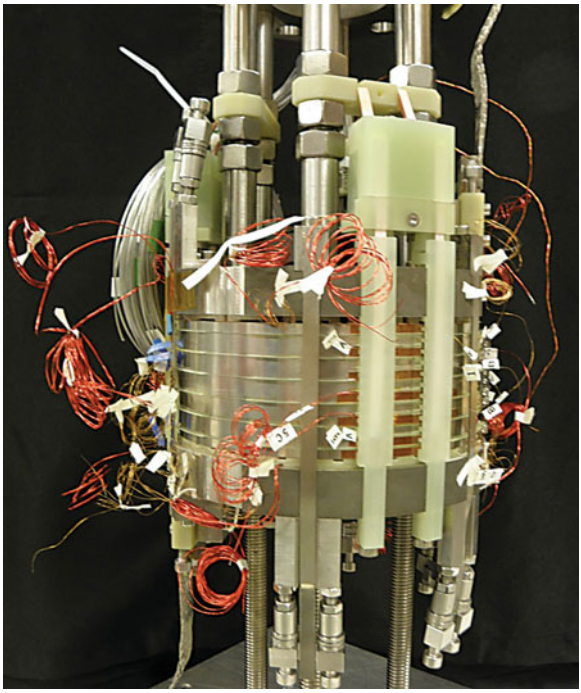

Fig. 7.25 A photograph of the 6-module prototype of coil 1 of the 32 mm bore multi-section 32 T showing the support structure and the instrument wiring [28] (*Courtesy*, H.W. Weijers, W. D. Markiewicz and D.C. Larbalestier, National High Magnetic Field Laboratory)

Table 7.6 Important parameters of the 32 T magnet (data compiled from [4, 28])

Parameter	Unit	Value
Working cold bore	mm	32
Total central field	T	32
Outer dia. of the HTS outer coil(2)	mm	232
Field by inner HTS coil (1) @ 180 A	T	11.0
Field by outer HTS coil (2) @ 180 A	T	6.4
No. of modules in coil (1) and coil (2)		20 and 36
Dimensions of REBCO tape conductor	mm × mm	4.1 × 0.17
Piece length for coil 1 and coil 2	m	60 and 110
Total conductor length used in coil (1)	m	2,758
Total conductor length used in coil (2)	m	6,621
Background field by Nb–Ti/Nb_3Sn coils	T	15.0
Operating current	A	180
Maximum conductor current density	A/mm^2	334
Maximum ramp rate (0–180 A)	A/sec	1
Maximum hoop stress	MPa	297
Design hoop stress	MPa	400

consists of 20 modules of double pancakes. The outer HTS coil has an inner dia. 164 mm and an outer dia. of 232 mm and consists of 36 double pancake modules. These dimensions are good enough to accommodate a dilution refrigerator. Availability of such high field and mK temperature range will undoubtedly open new frontiers of research in condense matter physics.

The HTS conductor is the coated tape of the size about 4.1 mm × 0.17 mm uninsulated. The tape conductor is co-wound with an insulated SS insulated tape which provided turn to turn insulation as well as mechanical strength through reinforcement. A double layer of G-10 provides module to module insulation and also sandwiches the encapsulated heaters used for quench protection. The inner and the outer HTS coils generate a field of 11 and 6.4 T respectively at an operating current of 180 A. The total stored energy in the two coils is 267 kJ and another 1.06 MJ is added due to the mutual inductance of the HTS coils and the LTS coils. The LTS magnet system along with the cryostat will be supplied by Oxford Instruments. The design allows the use of the LTS magnet system in stand-alone mode providing a field of 15 T in 250 mm cold bore. Both the magnet systems the REBCO and the LTS run on two separate power supplies and protected independently against quench.

The design of such magnet needed a vast amount of data on the conductor behaviour under extreme conditions of field, operating current and mechanical stresses, which was just not available. Quench protection to save the magnet at such high fields becomes a challenge. For stable fields extremely low resistance joints need to be developed. Since no such data existed, thorough studies were undertaken by FSU to generate first time data on numerous parameters crucial to the design of such a magnet.

The studies were aimed at investigating J_c/B behaviour of HTS at 4.2 K and variation of J_c with field, temperature, strain and field orientation. These parameters are critical to the magnet design. Crucial and unique to HTS, is the variation of J_c with field orientation. At the magnet ends, the field lines curve and make an angle with the direction of the field. J_c decreases with the angle and this variation has to be found out. It turns out that the limiting operating current of the inner HTS coils is not determined at high field mid-plane but at the magnet end. In this particular magnet design the field orientation angle is 18° at the magnet edge. A mathematical model [29] has been developed to study angular dependence of the J_c of REBCO tape under high magnetic field.

These studies have brought out interesting facts about HTS needed for magnet construction. These are summarized below.

- REBCO tapes have good irreversible strain of 0.6 % which stays at the lap joints of the tape if the overlapping length is more than 60 mm. For a given strain value the stress decreases as the amount of copper layer is kept 40–100 μm thick on a 50 μm thick Hastelloy tape. The tape also becomes soft with the addition of copper.
- The bare HTS tapes and wires supplied by the manufacturers need suitable electrical insulation. Metal oxide, UV-cured epoxy and Kapton have been

studied. The SS co-wind with a turn insulation was found to be a good winding technique. Sol-gel and UV cured epoxy have been found good as turn insulation on the SS strip. SS co-wind not only enhances mechanical strength but makes tape handling far more easier.

- Dry winding in double pancake structure involving number of steps and a large number of joints has been followed successfully. The winding is quite convenient as the REBCO tapes possesses large bending strain tolerance.
- The coils were operated at an average current density of 1.8 to 2×10^4 A/cm^2 (taking into account conductor thickness, copper fraction, inter pancake spacers and SS co-wind).
- The maximum stress in the winding was 400 MPa and the maximum strain 0.4 %.
- Winding lengths of the coils are determined as per the field and field uniformity requirement. Longer winding also cuts down radial component of the field. Inner coil uses a conductor length of 150 m per module and the outer coil 220 m.
- Passive quench protection system, good for LTS magnets, is no good for HTS because of the very low quench propagation velocities, high operating current densities and current sharing temperatures. The quench protection is provided by heaters distributed throughout the coils which have been found to be most effective. A quench detector activates the protective heaters the moment a quench is detected. Outer LTS coils have usual passive protection of resistors and diodes.
- The outer LTS coils and the inner HTS coils run on two separate power supplies.

After these exhaustive studies the magnet coils were designed, reduced-height prototypes fabricated and finally tested experimentally. The prototype coils have been successfully operated at current values higher than needed for 32 T field. It is expected that 32 T magnet will soon be a users' facility which will serve the world community for next 20 years or more.

7.9 Cryo-Free Superconducting Magnets (CFSM)

The biggest fall-out of the discovery of high temperature superconductors was the development of HT current leads capable of transporting large currents without Joule heating when operated below T_c. This development together with the availability of two stage Gifford-McMahon (GM) closed cycle refrigerator (CCR) of 1.5 W @ 4 K capacity led to the development of CFSM producing high fields. The HTS current leads have the twin advantage, one that there is no Joule heating across the leads and two that they behave nearly like a thermal insulator as superconductors have poor thermal conductivity, about 500 times smaller than OFHC. Since there is no hassle of producing and transferring liquid helium to the system, these

magnets have found wide spread popularity in a short time. A world record of 27.5 T by a hybrid magnet using a cryo-free outsert and the resistive magnet as an insert was established by IMR, Tohoku University, Sandai some years ago. Presently, CFSM producing field up to 20 T are available in the market.

The feasibility of a cryo-free magnet was reported by Hoenig [30] in 1983 who produced a field of 3.3 T using Nb_3Sn conductor and a 10 K two stage CTI-1020 CP Cryodyne cryocooler. This 12 kg Nb_3Sn magnet was operated at 14 K and produced a field of 3.3 T at a current density of 6×10^4 A/cm^2. It was, however, during 1990s when the HTS current leads became commercially available that massive development of CFSM, the world over, took place. There are numerous publications on CFSM we will just mention a few of them. A 6 T, 220 mm wide bore (room temperature) CFSM has been built by Watazawa et al. [31] using two sections of Nb–Ti coils. The weight of the magnet was 120 kg and had two sections. The inner section produces a field of 1.4 T and the outer section 4.6 T, both operating at a current of 152 A. Bi-2223 tubular current leads (ID = 20 mm × OD = 23 mm) have been used between the first and the second stage of the CCR. Two 4 K, GM cryocoolers were used to cool down the system. At the operating current of 152 A the heat load at the first stage turns out to be 42.8 W and 0.61 W at the second stage. The respective temperature at the two stages are 45 and 4.9 K. The magnet had an inductance of 35 H and a stored energy of 400 kJ.

Watanabe et al. [32] built a 52 mm room temperature bore CFSM which produced a field of 11 T. This magnet was the combination of an outer Nb–Ti coil and an inner Nb_3Sn coil and uses Bi-2223 current leads (same as in [31]). The magnet was cooled by a pair of 4 K GM cryocoolers. The coils were operated at 6 K at a current of 150 A which generated a central field of 11 T. The magnet parameters are given in Table 7.7. Each coil is protected against quench by a pair of diodes and a resistor of 2.9 Ω placed close to the respective coil. During the quench about 35 %

Table 7.7 Parameters of a 11 T cryo-free superconducting magnet (data compiled from [32])

Parameter	$(Nb, Ti)_3Sn$	Nb-47 wt% Ti
Conductor dimensions	0.9 mm (dia)	0.76 × 1.5 mm
No. of filaments	54	1,050
Filament dia.	90 μm	22 μm
Cu: SC ratio	0.87	1.9
Coil inner dia.	86 mm	187 mm
Coil outer dia.	177 mm	281 mm
Coil height	222 mm	225 mm
Operating temp.	6 K	6 K
Operating current	150 A	150 A
Field generated	6.4 T	4.6 T
RT Bore	52 mm	
Total central field	11 T	
Total inductance	19 (H)	
Total stored energy	215 kJ	

of the total stored energy of 215 kJ is adiabatically absorbed by the magnet system and the protective diode-resistor system. Coil temperature rises by 50 K. The magnet was charged up to 130 A at a ramp rate of 3 A/min, up to 140 A at 2 A/min and finally at 1 A/min up to 150 A. The ac loss mainly comes from the hysteresis in the superconductor and is of the order of 30 mW. The equilibrium temperatures at a field level of 10.5 T are, 4.8 K for both the coils, 4.7 K at the cold end (stage II) of the cryocooler and 59 K at the warm end of the current leads.

Of late, pulse tube cryocoolers (PTC) with 1.5 W cooling capacity have become commercially available. PTC have the advantage that there is no moving part in it like the displacer in the GM cryocooler. They are thus free from mechanical vibrations and from electromagnetic noise. These PTCs are preferred for experiments where vibrations are not acceptable and the noise level has to be small. Secondly, the life cycle is going to be much higher than 10,000 h. of free maintenance of the GM cryocoolers. The PTCs do consume large power in so far as about 6.5 kW power is required to produce 1.5 W of cold compared to 0.25 to 1 kW power required to produce 1 W of cooling by liquid helium. This cost is, however, more than off-set by net saving in helium cost and heavy investment if one has to install helium liquefaction facility.

A 5 T Nb–Ti magnet with room temperature bore of 50 mm was built by Giebeler et al. [33] in 2004 using a two stage PTC with a cooling capacity of 0.4 W @ 4.2 K. It is a compact 12 kg magnet, 190 mm in height and produces a field of 5 T at a charging current of 35 A. The PTC cools down the magnet to 2.7 K in 44 h. The minimum temperature attained is 2.4 K. The temperature stability at the first and second stage are 5 and 0.1 K respectively over a period of 21 days. The magnet runs in persistent mode. The persistent switch is cooled by the second stage of the PTC.

We would like to take-up the design and operation of a CFSM a bit in detail now. As an example, we again take up the construction of our own 6 T, 50 mm room temperature magnet which we built at our centre some years ago. Before we do that, let us discuss the crucial issues involved in the design and operation of a cryo-free magnet and which are generally not reported being a propriety item of the manufacturers.

7.9.1 Important Considerations for CFSM System Design

- The most important and foremost issue is that there is no longer a liquid helium bath which has large capacity to cool the magnet and absorb heat rather quickly. Cryo-free magnets are cooled by the second stage of the CCR through thermal conduction which is a slow process and depends upon the quality of the thermal contacts. A small thermal disturbance, if not dissipated to the CCR fast enough, may raise the temperature locally and quench the magnet.
- A thermal analysis of all heat loads to the two stages of the CCR must be carried out carefully before embarking on the design. Total heat loads should be reasonably below the refrigeration capacity of the two respective stages.

- The thermal shield and the magnet, the two heaviest components of the whole system, are cooled by the first stage and the second stage of the CCR respectively by thermal conduction only. Thermal contacts have therefore to be nearly perfect with least thermal resistances.
- Flexible OFHC braids often serve ideal material for thermal connections whether fixed mechanically or through soldering. Flexibility prevents stresses in the system during thermal cycles.
- The magnet should preferably use former made of copper. The former must have perforations and should have a slit along the entire length (including flanges) to minimize the eddy current heating during ramp-up and ramp-down of the magnet.
- The magnet is cooled via the top and bottom flanges of the former in thermal contact with the second stage. Cooling of coil starts from the outer and inner layers. Inter-layers should be avoided as this will slow down the thermal conduction making the layer to layer heat transfer inefficient.
- We recommend wet winding using stycast epoxy mixed with 15–20 wt% aluminum nitride (ALN) powder. Wet winding ensures fool-proof impregnation and ALN powder improves the thermal conductivity of the stycast. ALN also reduces the mismatch of the thermal contraction coefficients of the epoxy and the conductor, minimizing cracking under Lorentz forces during cooling.
- Since there is no bath to keep the magnet temperature constant, operating temperature has to be estimated at the target field. The magnet temperature rises from the zero current state as the magnet current is ramped up. A good temperature margin (>1 K) should be maintained between the operating temperature and the current sharing temperature.
- The maximum heat to the system comes from the current leads. In CFSM the current leads are hybrid, a combination of copper leads from room temperature to thermal shield and HTS leads from shield to the magnet connected with the second stage of the CCR. Heat input to the thermal shield consists of heat conducted from the room temperature top plate and also due to Joule heating within the copper leads. The copper current leads therefore should be optimized for the operating current to minimize Joule heating.
- Between the shield and the magnet, the current leads are HTS leads generating practically no heat. These leads are joined to the copper current leads. These contacts should have very low electrical resistance to minimize Joule heating. These joints should be anchored to the shield through spacers of material like ALN which are not only good electrical insulator but also good thermal conductor. The lower ends of the HTS leads are connected to the magnet and the second stage of the CCR.
- The performance of the CCR and the HTS leads deteriorate in presence of the magnetic field. A field profile of the magnet should therefore be carried out in advance so that the HTS leads and the CCR heads are positioned in low field areas where the stray field is below 0.1 T.
- An efficient quench protection system similar to one used with the bath-cooled magnets has to be designed such that the magnet temperature does not exceed

40–50 K after the quench. In these systems there is no helium gas pressure build-up at quench in contrast with the bath-cooled magnets.

7.9.2 The Design and Winding of the Magnet

To discuss the construction details of a CFSM system, we take up the example of a 6 T, 50 mm warm bore Nb–Ti magnet we built [34, 35] in our laboratory. The design considerations for the bore dia., field strength, current and number of turns and layers are the same as for any bath-cooled magnet, discussed in detail in Sect. 7.4. The major consideration here is that the operating temperature of the magnet is to be calculated from heat loads coming to the magnet from different sources for the given field, the three critical parameters of the conductor, T_c, J_c and B_{c2} being inter-dependent. The operating current is then chosen from the conductor I_c-B plots.

To have a warm bore of 50 mm we chose the inner winding dia. of 104 mm and a winding length of 200 mm on the basis of field homogeneity criterion. The outer winding dia.comes out to be 137 mm. At an operating current of 102 A the magnet should produce a field of 6 T. This current is 68 % of the short sample I_c value supplied by the manufacturer. We emphasize that the J_c and B_{c2} values quoted are at 4.2 k and at zero current. Similarly, T_c value is always quoted in zero field and zero current. For CFSM we have to find out the current sharing temperature, T_{cs} which is higher than zero current T_c. The current sharing temperature, T_{cs} is defined as the temperature at which the current starts flowing partly through copper. As the magnet current rises T_{cs} too starts rising. The temperature window to operate magnet becomes narrower. Values of T_c and T_{cs} can be estimated at different fields using following equations given by Lubell [36].

$$T_c(B) = T_c(0) - [1-(B/14.5)]^{0.59} \tag{7.19}$$

$$T_{cs}(B) = T_b + [T_c(B) - T_b]\left(1-J_{op}/J_c\right) \tag{7.20}$$

where $T_{cs}(B)$ is the current sharing temperature at a field B, T_b the operating temperature, J_{op} the operating current and J_c the critical current. The T_{cs} values and also the temperature margin for operating the magnet at 6 T field has been evaluated for different operating currents and are listed in Table 7.8. For an operating current of 102 A and an operating temperature of 4.2 K the T_{cs} for this 6 T magnet is 5 K. Thus the temperature margin ΔT is only 0.8 K. However if the magnet is operated at 3.3 K the ΔT goes up to 1.7 K. The T_c of Nb–Ti at 6 T is 6.71 K. The operating temperature should therefore be as low as feasible by reducing the heat leaks to the two stages of the CCR to a minimum. T_{cs} thus becomes an important input parameter for the magnet design calculations,

Table 7.8 Current transfer temperature T_{cs} at 6 T and different operating currents and the temperature margin, ΔT for Supercon 0.54 mm dia. Nb–Ti wire with I_c = 150 A @ 6 T, 4.2 K

Operating current (A)	% of I_c	T_b (K)	$T_c(B)$ at B = 6 T (K)	T_{cs} (K)	$\Delta T = T_{cs}–T_b$ (K)
50	33.3	4.2	6.71	5.86	1.67
90	60	4.2	6.71	5.204	1.0
102	68	4.2	6.71	5	0.8
135	90	4.2	6.71	4.45	0.25
150	100	4.2	6.71	4.2	0

The magnet is wound on a electro-tough pitch (ETP) copper former with a slit along the entire length. The slit reduces heat generation due to eddy current induced in the former during charging and discharging of the magnet. A layer of thin Kapton tape was wrapped on the former surface to make it electrically insulating. Supercon 0.54 mm dia. Cu/Nb–Ti wire was used for coil winding. We preferred wet winding using stycast epoxy mixed with ALN (aluminum nitride) powder as filler to improve it's thermal conductivity and reduce mismatch in thermal contraction values of the epoxy and the conductor. Since the cooling of the coil proceeds layer to layer, no inter-layer has been used which would have hampered layer to layer conductance. All the parameters of the magnet are given in Table 7.9.

Table 7.9 Parameters of a 50 mm warm bore CFSM built at author's laboratory [34, 35]

S. no.	Magnet parameter	Unit	Value
1.	Inner winding dia.	mm	104
2.	Outer winding dia.	mm	137
3	Winding length	mm	200
4	Inter-layer		None
5	Impregnation (wet winding)		Stycast with filler
6	Conductor used		MF Cu/(Nb–Ti)
7	Wire dia.	mm	0.54
8	No. of filaments		54
9	Filament dia.	μm	38
10	Cu/Nb–Ti ratio		2.0 ± 0.2:1
11	Total conductor length	km	4.1
12	No. of layers		32
13	No. of turns/layer		370
14	Peak field	T	6.2
15	Current at peak field		105.3
16	Field factor (T/A)		0.0588
17	Stored energy at peak field	kJ	31.04
18	Quench protection (dump resistor)	Ω	0.5

7.9.3 Current Lead Design

The optimization of the copper part of the hybrid current leads is crucial in so far as it determines the heat input to the top plate of the thermal shield and its temperature. This directly affects the minimum temperature reached at the second stage and hence the operating temperature of the magnet. Please remember that there is no helium vapour cooling available like in bath cooled magnets. Optimization of conduction cooled current leads can be done using following equations given by the McFee model [37].

$$\frac{Q_{\mathrm{OPT}}}{I} = \sqrt{L_0\left(T_W^2 - T_C^2\right)} \tag{7.21}$$

$$\left(\frac{IL}{A}\right)_{\mathrm{OPT}} = \frac{1}{\sqrt{2}} \int_{T_c}^{T_W} \frac{k(T)dT}{\sqrt{L_0\left(T_W^2 - T_c^2\right)}} \tag{7.22}$$

where Q_{OPT} is the optimized heat flow, L_0 the Lorenz number, T_W and T_c are the temperatures at the warmer end and the colder end of the copper lead respectively. I is the lead current, L and A are the length and the area cross-section of the lead respectively. $k(T)$ is the temperature dependent thermal conductivity of the lead material. Using (7.21) Q_{OPT} for a lead carrying current between 300 and 33 K comes out to be 47 mW/A. Substituting appropriate values of the different parameters, in (7.22) the lead parameter, IL/A for copper of RRR 150 purity turns out to be 4.5×10^6 A/mm^2. Thus for a current lead of area cross-section 15 mm^2 and optimized for 85 A, the length should be 800 mm. Calculations show that for values of RRR 50 to RRR 300 the lead parameter is same at all temperatures from 300 K down to 30 K.

7.9.4 The Cryostat Design

The CFSM system is schematically shown in Fig. 7.26 which basically consists of a wide body SS vacuum chamber. The CCR sits off-the-centre on the top plate of the chamber. The top plate of the cylindrical thermal shield, made out of ETP copper, was suspended from the top plate of the chamber using G-10 strips. This plate is thermally connected to the first stage of the CCR using copper braids. Indium gaskets have been used at all the contact interfaces to reduce thermal resistance. The magnet is mounted on a slotted ETP copper plate which is thermally anchored, mechanically, to the cold head of the second stage of the CCR through sixteen semi flexible copper strips (20 mm × 2 mm). Apiezon N grease mixed with copper powder is used at the interface to improve thermal conduction. The magnet, weighing about 15 kg, is supported by G-10 strips from the top of the shield as

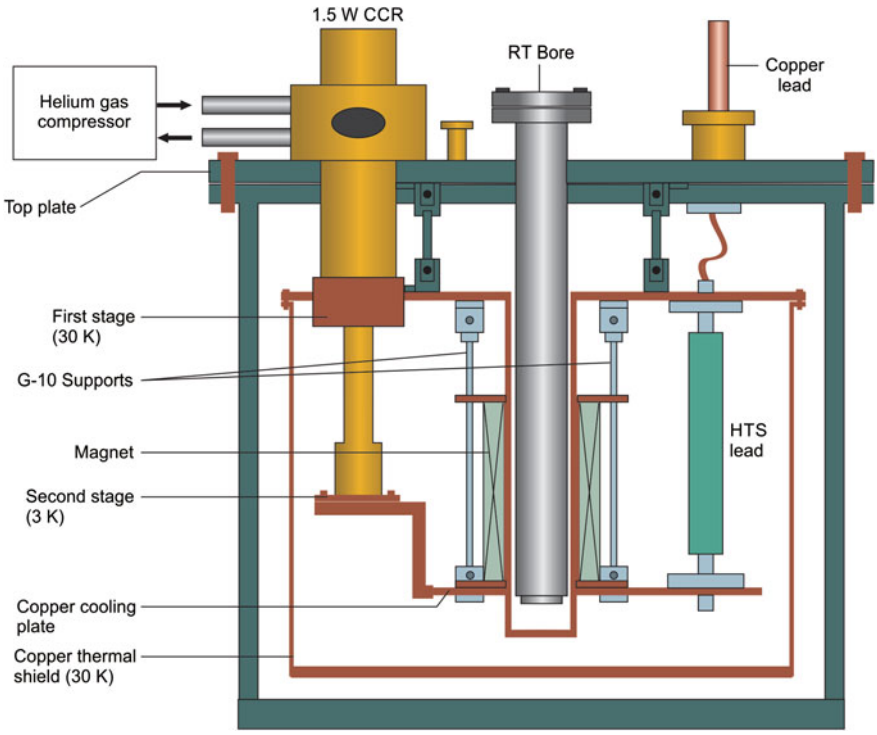

Fig. 7.26 A schematic diagram of a 6 T CFSM system built in author's laboratory at IUAC [34, 35]

shown in Fig. 7.26. The total thermal mass directly cooled by the second stage cold head is about 17 kg which consists of the former, Nb–Ti coil and the heat transfer plate. A pair of hybrid current leads. consisting of pure copper leads in the warmer region (between top plate and the shield) and HTS leads in the colder region (between shield and the magnet) are used to charge the magnet. The copper part of the leads was optimized for an operating current of 102 A between 300 and 35 K using Mcfee model [37]. The dimensional parameter, (*IL*/*A*) for copper of RRR 150 turns out to be 4.4×10^{-6} A/mm^2. For a 15 mm^2 cross-sectional area the length of the lead has to be 650 mm. The heat load per lead works out to be 4.7 W. It is a good idea to simulate the experiment in advance with a dead mass of weight equal to the magnet and find out the different heat loads static and dynamic with and without the magnet current. This will help to know the temperature of the shield and optimize the copper current leads correctly. We carried out such simulation for this magnet [38]. The complete assembly of the system is shown in Fig. 7.27. The entire system hangs from the top plate of the vacuum chamber. Copper current leads (in braid form) are joined with the copper braid terminals of the HTS inside a copper bush with lead-tin solder. These joints are thermally anchored to the top plate of the thermal shield and electrically insulated through the use of ALN disc spacers.

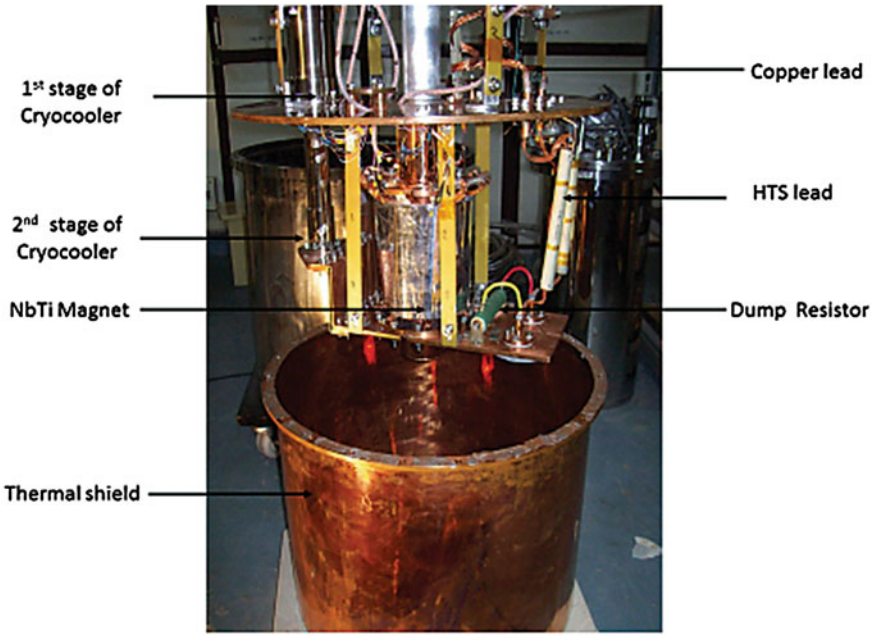

Fig. 7.27 The photograph of the inner assembly of the 6 T CFSM built at IUAC. The top plate of the vacuum chamber and thermal shield, HTS current leads and shield chamber, are visible (*Courtesy* IUAC Delhi)

Similarly, the lower ends of the HTS leads (copper braids) are soldered to Nb–Ti wire terminals and anchored to the heat transfer plate using same type of copper block and ALN spacer. This plate is already thermally connected with the second stage of the CCR.

Figure 7.28 is the photograph of the complete CFSM system with central RT bore and all feed thrus. The Bi-2223 HTS leads, (model CSL-7/120.1) were bought from CAN Superconductors. The conductive heat leak through the lead pair between 64 and 4 K is 20 mW. Silicon diode temperature sensors have been mounted at several locations of the system to monitor temperature for carrying out thermal analysis later.

7.9.5 Operating the Magnet

It is advisable to test the magnet and train it in a liquid helium bath cryostat before being installed in the cryo-cooled chamber. This 6 T magnet was tested in bath cryostat and energized at a slow rate 3A/min. The first quench occurred at 80.1 A (4.7 T), second at 87.2 A (5.15 T) and third at 99 A (5.85 T). Finally, the magnet produced a field of 6.2 T at a current of 105.2 A without quench. After the training,

Fig. 7.28 The photograph of the complete CFSM system with central RT bore and all feed-thrus (*Courtesy* IUAC Delhi)

the magnet was charged at a sweep rate of 30 A/min to 6 T without quench. The B-I_{op} data obtained and quench positions are plotted in Fig. 7.29. After the magnet was tested and trained up to 6 T it was dismounted from the test cryostat and was transferred to its new destination within the vacuum chamber. The performance details can be found in [39]. All the components of the system in the final configuration are shown in Fig. 7.27. After ensuring all the lead connections, proper mounting of the thermal transfer plates to the two stages of the CCR, the vacuum chamber was evacuated to 10^{-5} mbar. The magnet cools down to a minimum of 3.3 K in 15 h. The vacuum at this temperature improves to 10^{-9} mbar. The equilibrium temperatures of the cold head, magnet cooling plate and the copper anchor recorded are 2.75, 3.1 and 4.5 K respectively. The difference between the temperatures of the cold head and the outer layer of the magnet is only 0.6 K. The thermal shield temperature stabilizes at 35. 7 K.

The magnet was energized in steps of 10 A at a ramp rate of 3 A/min. up to 102 A corresponding to the field 6 T. Magnet quenched at 87 A and 102 A during the first run of this system. Temperature of the magnet rose to 41.5 and 54 K after the quench at the two current values respectively. Magnet, however, cools down to

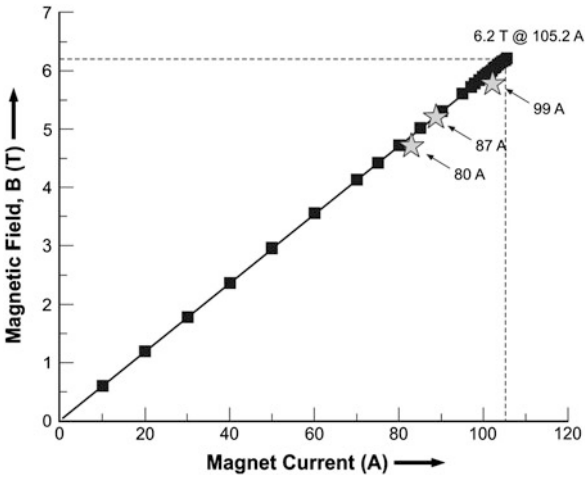

Fig. 7.29 Training of the magnet in liquid helium bath. Maximum field produced 6.2 T @ 105.2 A. Magnet quenched at 80, 87 and 99 A during training [39]

3.3 K, the operating temperature in just 40 min. We find the maximum workable ramp rate to be 6A/min. Beyond this value the heat generation caused by the AC losses and the induced eddy currents exceeds the heat extraction rate of the CCR. This is because of the inherent thermal resistances at the current lead joints. At 102 A current the magnet stabilizes at 4 K and the cold head at 3.13 K. Temperature at the lower end lead joint too goes from 4.5 to 6.6 K at 102 A. This temperature rise is due to the Joule heating of the copper braid which connects the HTS lead with the magnet. With a resistance of 10 μΩ the braid generates 210 mW of heat at 102 A. Estimates show that static heat load at the first stage without lead connection is only 14.6 W and goes up to 19.8 W after lead connections but no current and to 25.3 W at 102 A in the leads.

An elegant and systematic electro-thermal analysis of the heat load transferred to the two stages of the CCR by various sources has been carried out by Kar et al. [40]. The entire magnet system from room temperature to magnet has been reduced to a network of electrical and thermal resistances as detailed in Fig. 7.30. Electrical contact resistances of all the joints were measured experimentally. Thermal resistances were calculated from the measured temperatures at appropriate places and using thermal conductivity of the material. It turns out that the heat input to the first stage comes mainly from the optimized copper current leads followed by warm end cu-braid, Cu–Cu joints and Cu–HTS joints. All these heat inputs show an increase with magnet current. Similarly high heat input to the second stage comes from heating of the lower copper braid, followed by Cu–HTS joints and Cu–Nb–Ti joints, all again going-up with the increase of magnet current. Heat generated in HTS leads is less than 5 mW and stays current independent.

Above discussion clearly establishes the fact that it is extremely important to design the hybrid current leads meticulously so that the heat inputs to the two stages of the CCR are well within their cooling powers. All the inter-lead joints should have low contact resistance producing minimum heat. Anchoring to thermal shield

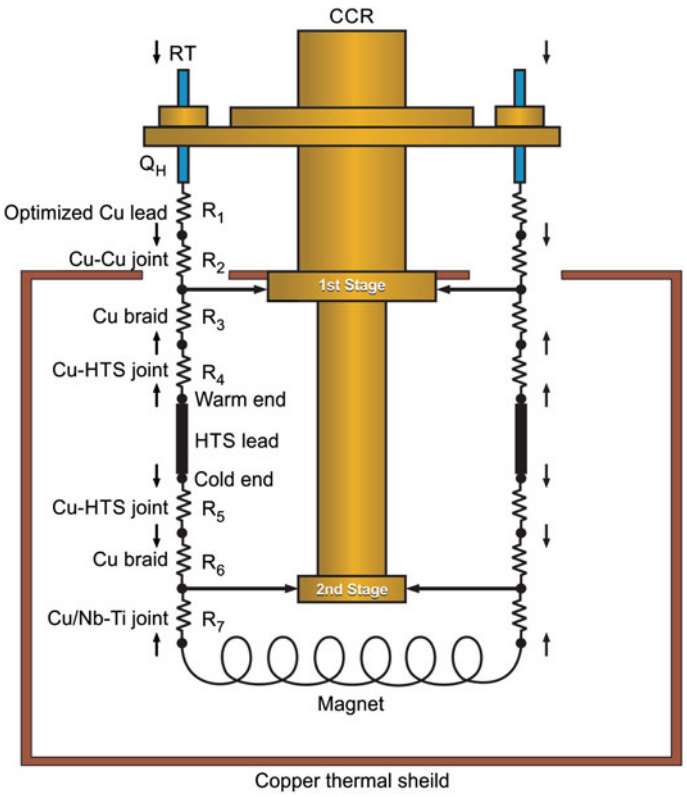

Fig. 7.30 The resistance network model used to calculate heat loads to the first and second stage of the CCR, generated by various resistances and joints [38]

and magnet cooling plate have to be perfect. Technology to built cryo-free magnets producing field up to 20 T is well established by now. Looking at the great developments that are taking place in the production of superior quality HTS conductors in long lengths and similar development in high power CCRs, a day is not far when cryo-free magnets producing 30–50 T field will be a reality and much sooner than expected.

References

1. G.B. Yntema, IEEE Translations on Magnetism, **MAG-23**, 390 (1987)
2. H.T. Coffey, J.K. Hulm, W.T. Reynolds et al., J. App. Phys. **36**, 128 (1965)
3. J.E. Kunzler, E. Buehler, F.S.L. Hsu, J.H. Wernick, Phys. Rev. **6**, 89 (1961)
4. W.D. Markiewicz, D.C. Larbalistier, H.W. Weijers et al., Magnet Technology, MT-22, 2CO-8, (2011), IEEE Trans. App.Supercond., **22**, 4300707 (2012)

5. U.P. Trociewitz, M. Dalban-Canassy, M. Hannion et al., Appl. Phys. Lett. **99** (20), 202506 (2011)
6. Ulf P. Trociewitz, M. Dalban-Canassy, M. Hannion et al., 35.4 T field generated using a layer-wound superconducting coil made of (RE)$Ba_2Cu_3O_{7-x}$ (RE = Rare Earth) coated conductor, http://arxiv.org/ftp/arxiv/papers/1110/1110.6814.pdf
7. R.W. Boom and R.S. Livingston, Proc. IRE **50**, 274–285 (1962)
8. Ch. Fabry, L'Eclairage Electrique **17**, 133 (1898)
9. Ch. Fabry, J. Phys. **9**, 129 (1910)
10. D.B. Montgomery, *Solenoid Magnet Design* (Wiley, New York, 1969)
11. H. Brechna, *Superconducting Magnet System* (Springer, New York, 1973)
12. M.N. Wilson, *Superconducting Magnets* (Clarendon Press, Oxford, 1983, 1986, 1989)
13. Y. Iwasa, *Case studies in Superconducting Magnets- Design and Operational Issues* (Plenum Press, New York, 1994)
14. K.H. Mess, P. Schmüser, S. wolff, *Superconducting Accelerator Magnets* (World Scientific Hemberg, 1996)
15. S. Kar, Rajesh. Kumar, Manoj Kumar et al., Ind. J. Cryo. **32**, 131 (2007)
16. B.J. Maddock, G.B. James, Proc. IEE **115**, 543 (1968)
17. Rajesh Kumar, S.K. Suman, A. Mandal, INPAC -2011, http://www.iuac.res.in/InPAC2011/proceedings/InPAC2011%20Proceedings/poster16Feb2011.html
18. R.G. Sharma, Y.S. Reddy, R.B. Saxena et al., in *A Superconducting Magnet System for 100 MHz NMR Spectrometer, Advances in Instrumentation* eds. by B.S. Ramprasad, S. Ashokan, K. Rajanna, N.C. Shivaprakash. Proceedings of International Conference Instrumentation (ICI-1996), August 8-10, Bangalore, India
19. T. Kiyoshi, M. Kosuge, K. Innoue, H. Maeda, Phys. B **216**, 196 (1996)
20. R.G. Sharma, Y.S. Reddy, M.M. Krishna et al. *News item NPL Develops Nb_3Sn Magnet Technology* (NPL (India) Technical Bulletin, April 1992), p. 14
21. R.G. Sharma, R.B. Saxena, M.A. Ansari, *An 11 T Nb–Ti/Nb_3Sn Magnet* (Research Report, NPL (India), 2003)
22. K. Tachikawa, Y. Tanaka, K. Inoue et al., 17.5 Tesla Superconducting Magnet. J. Cryogenic Soc. Japan **11**, 252 (1976). (in Japanese)
23. M. Oshikiri, K. Inoue, T. Kiyoshi et al., Phys. B **201**, 521 (1994)
24. T. Kiyoshi, K. Inoue, K. Itoh et al., IEEE Trans. App. Super. **3**, 78 (1993)
25. T. kiyoshi, M. Kosuge, K. Inoue, H. Maeda, Physica, **B 216**, 196 (1996)
26. S. Matsumoto, T. Kiyoshi, A. Otsuka et al., Supercond. Sci. Technol. **25**, 025017 (2012)
27. D. Larbalestier, New Magnet Lab. record promises more to come, News and press releases, August 7, 2007 www.magnet.fsu.edu/mediacenter/news/pressreleases/2007august7.html
28. H.W. Weijers, W.D. Markiewicz, A.J. Voran et. al., IEEE Trans. App. Supercond. **24**, 5 (2013)
29. D.K. Hilton, U.P. Trociewitz, H.W. Weijers, D.C. Larbalestier (FSU, To be published)
30. M.O. Hoenig, IEEE Trans. Magn. **MAG**-19, 880 (1983)
31. K. Watazawa, J. sakuraba, F. Hata et al., IEEE Trans. Magn. **MAG-32**, 2594 (1996)
32. K. Watanabe, S. Awaji, J. Sakuraba et al., Cryogenics, **36**, 1019 (1996)
33. F. Giebeler, G. Thummes, K-J. Best, Supercond. Sci. Technol. **17**, S-135 (2004)
34. S. Kar, P. Konduru, R. Kumar et al., Advances Cryo. Engg. **57A**, 597 (2012)
35. S. Kar, P. Konduru, R. Kumar et al., Advances Cryo. Engg. **57A**, 909 (2012)
36. M.S. Lubell, IEEE Trans. Magn. **19**(3), 754 (1983)
37. R. McFee, Rev. Sci. Instrum. **30**, 98 (1959)
38. S. Kar, A. Chaudhury, P. Konduru et al., Ind. J. Cryog. **35**, 246 (2010)
39. P. Konduru, S. Kar, M. Kumar et al., Ind. J. Cryo. **36**, 81 (2011)
40. S. Kar, P. Konduru, R.G. Sharma et al., IEEE Trans. Appl. Super. **23**, 4800507 (2013)